IEEE Access
Multidisciplinary | Rapid Review | Open Access Journal

Received December 8, 2021, accepted December 27, 2021, date of publication December 30, 2021,
date of current version January 12, 2022.

Digital Object Identifier 10.1109/ACCESS.2021.3139341

Control of LPV Modeled AC-Microgrid Based on Mixed H_2/H_∞ Time-Varying Linear State Feedback and Robust Predictive Algorithm

MOSLEM DEHGHANI[1], MOHAMMAD GHIASI[1,2], (Member, IEEE), TAHER NIKNAM[1], (Senior Member, IEEE), KUMARS ROUZBEHI[3], (Senior Member, IEEE), ZHANLE WANG[2], (Member, IEEE), PIERLUIGI SIANO[4,5], (Senior Member, IEEE), AND HASSAN HAES ALHELOU[6,7], (Senior Member, IEEE)

[1]Department of Electrical and Electronic Engineering, Shiraz University of Technology, Shiraz 71555-313, Iran
[2]Electronic Systems Engineering, University of Regina, Regina, SK S4S 0A2, Canada
[3]Department of Systems Engineering and Automatic Control, University of Seville, 41004 Seville, Spain
[4]Department of Management and Innovation Systems, University of Salerno, 84084 Salerno, Italy
[5]Department of Electrical and Electronic Engineering Science, University of Johannesburg, Johannesburg 2024, South Africa
[6]Department of Electrical Power Engineering, Tishreen University, Lattakia, Syria
[7]Department of Electrical and Computer Systems Engineering, Monash University, Clayton, VIC 3800, Australia

Corresponding authors: Hassan Haes Alhelou (alhelou@tishreen.edu.sy) and Taher Niknam (niknam@sutech.ac.ir)

ABSTRACT This paper presents a robust model predictive control (RMPC) method with a new mixed H2/H∞ linear time-varying state feedback design. In addition, we propose a linear parameter-varying model for inverters in a microgrid (MG), in which disturbances and uncertainty are considered, where the inverters connect in parallel to renewable energy sources (RES). The proposed RMPC can use the gain-scheduled control law and satisfy both the H2 and H∞ proficiency requirements under various conditions, such as disturbance and load variation. A multistep control method is proposed to reduce the conservativeness caused by the unique feedback control law, enhance the control proficiency, and strengthen the RMPC feasible area. Furthermore, a practical and efficient RMPC is designed to reduce the online computational burden. The presented controller can implement load sharing among distributed generators (DGs) to stabilize the frequency and voltage of an entire smart island. The proposed strategy is implemented and studied in a MG with two DG types and various load types. Specifically, through converters, one type of DGs is used to control frequency and voltage, and the other type is used to control current. These two types of DGs operate in a parallel mode. Simulation results show that the proposed RMPCs are input-to-state practically stable (ISpS). Compared with other controllers in the literature, the proposed strategy can lead to minor total harmonic distortion (THD), lower steady-state error, and faster response to system disturbance and load variation.

INDEX TERMS Microgrid, linear parameter varying system, distributed generation unit, H_2/H_∞ control, robust model predictive control.

I. INTRODUCTION

In cases where power electricity consumption would be too far from the main power network, for instance, remote villages or isolated islands or communication stations, it will be technically difficult or economically inefficient to deliver power electricity through transmission lines. Under these circumstances, a logically and economically sound approach to the power supply is in the form of MG island mode, which includes RESs like photovoltaic (PV) generators, wind turbines, etc. In these islanding modes of MGs, the DGs in the MG are responsible for controlling the voltage, current, and frequency alone and without any assistance from the main power network [1]–[3]. As a result, it is vital to plan and design a proper and suitable controller that is robust against MG's disturbances and also load variations. In this regard, one of the main aims of this article would be to present a robust non-linear controller for MGs. To reach this goal, several control approaches were used for MGs. For instance, master-slave control mode, and current control mode, or droop control have been used in references [4]–[6]. These approaches need communication plans, except for the

The associate editor coordinating the review of this manuscript and approving it for publication was Bin Zhou.

droop controllers, which have attracted a lot of attention for MGs. However, the operating of inverters with droop control can have some problems like voltage-frequency and current control responses, which are excessively and unpleasantly slow or might have a small or uncertain stable operational range [7].

A. BACKGROUND

To tackle the mentioned problems, some articles have proposed different approaches by using modifications of phase feedforward, droop control by first-order dynamics, as well as output impedance control of inverters [8]. However, modification strategies usually do not consider dynamic control of a system with order greater than one or dynamic control of gain scheduled, and also do not utilize progressive methods to control the plan, schedule, and design in a grid. Recent articles have demonstrated the benefits of robust controllers in comparison with common controllers according to traditional control theory to control the applicability of inverters in an MG [9]. In the reference [10], for instance, authors have demonstrated that the operational range of an MG might be risen from 6 percent to 14 percent for changing in all characteristics of a system. For example, in inverter voltages, or line impedances, one utilizes a dynamic control for the grid rather than a fixed gain droop controller. Although this could be remarkable progress, MGs might be subject to several variations and uncertainty; thus, other solutions and methods are required. Subsequent advances in efficiency and stable operational range might be considered via utilizing adaptive gain scheduled controllers. Progressions of 30 percent to 50 percent have been shown by using polytopic adaptive controllers in the paper [11]; nonetheless, such controllers are typically hard to implement and synthesize. The intricacy could be remarkably decreased for a small operating point with bumpless-transfer controllers that have appeared in works as an adaptive ad-hoc control plan [12], [13]. References [14], [15] have also stated that this method can be easier to synthesize, having less conservative, and also easier to perform in comparison with a polytopic controller and interpolation plan; besides, it would have a better operational range compared with a nominal and common type of controller. In such cases, whenever an inverter with an equal amount of impedance is connected to an MG that is much less than what is predicted by the design engineer, the inverter with a formal controller displays instability in responses and also the inverter with a bumpless controller displays stability in responses [11]. In the references [16], [17], for grid-supporting inverter-based systems, a new cascaded control strategy and a generalized droop control have been proposed where compared virtual synchronous generator control and traditional droop control.

Other approaches have also been utilized for (uninterruptable power supply (UPS) and DC/AC inverter systems, as those presented in the reference [18], where proportional-integral controllers have been utilized to track current and voltage references. A feedback linearization method was utilized for 3-phase UPS in the paper [19], where the control gains were obtained using a pole placement. Additionally, other alternatives dealing with advanced control methods can be found in the reference [20]; and also for adaptive controllers in reference [21], for sliding mode controllers and for model predictive controllers in the papers [22], [23]. It is noted that in the papers [24], [25], for power electronics applications, a robust control-based on linear matrix inequalities (LMIs) was addressed. The used strategy is attractive because it can be effectively solved by specialized algorithms, and also it allows for easily including many efficiency specifications. In this way, utilizing of LMIs for stability assessment and control design with practical performance for UPS deserves more investigation.

B. MOTIVATION AND MAIN CONTRIBUTIONS OF THE PAPER

In the islanding mode of MG, the voltage and frequency of the network should be constant. In this regard, in this article, one of the units is in the voltage-frequency control mode. To maintain the voltage and frequency of the network, other units that are not responsible for voltage-frequency control are in the current control mode. If the load current is more than the maximum current supplied by the current control unit, the current will be drawn from the current generation unit. The rest of the current is supplied by the voltage-frequency control unit. Also, if the load current is less than the maximum current of the current control unit, the total load current is supplied by the current control unit.

To enhance the control performance and feasibility of the presented method, in this paper, a mixed H_2/H_∞ feedback RMPC for systems with both disturbance and uncertainty structured is proposed. The multistep control approach is presented in the proposed mixed H2/H∞ RMPC, in which a sequence of feedback control laws is adopted as a control strategy. Besides this, since the ISpS concept is suitable to assess the stability of the closed-loop system with disturbance, the closed-loop ISpS stability is utilized to validate the proposed RMPC. Furthermore, a novel control strategy is introduced for islanding MG with different DGs according to a mixed H_2/H_∞ time-varying linear state feedback robust model predictive control algorithm to control voltage, current, and frequency of the power network system, and also for load sharing among DG units. Another important point in this work is to consider increasing the TDH and root mean square (RMS) value of the voltage profile of MG. One DG is working in the mode of voltage-frequency control; in this case, it will control the voltage and frequency in the power network by forcing the voltage of the grid to follow a reference signal simultaneously trying to lessen the error of output voltage. Similarly, another DG unit is operating in the mode of current control. The reference signal of the current is proportional to the load current that is measured on a real-time basis. The presented method is simulated and validated in different case studies using the MATLAB software.

C. PAPER STRUCTURE

The remainder of this manuscript is organized as follows; in Section II, the dynamic model and concept of the system and the proposed controller will be introduced and explained. In Section III, the results of the simulation of a low voltage MG will be provided and evaluated in different scenarios. Finally, remarks of conclusions will be presented in Section IV.

II. SYSTEM MODEL AND CONTROLLER DESIGN

A. SYSTEM MODEL

In this section, we present the concept of the proposed system. Figure 1 shows an islanded MG with different DG agents that are coupled to the AC bus in parallel mode. In the suggested system, one unit acts in voltage-frequency mode; in this case, it will be in the duty of stabling the MG voltage. The other unit is working in the current control mode and load sharing. Figure 2 depicts the circuit of a 3-phase inverter that is linked to the system. In this case, the output of the LC filter has been employed to decrease the output voltage of harmonic components produced by the pulse width modulation (PWM) inverter. The proposed case is operated in 2 different modes: voltage-frequency or current control mode. Each DG system is composed of LC filters, a DC resource, and a voltage source inverter in common conditions. The power circuit and control schematic diagram of a 3-phase inverter with LC filter is shown in Figure 3.

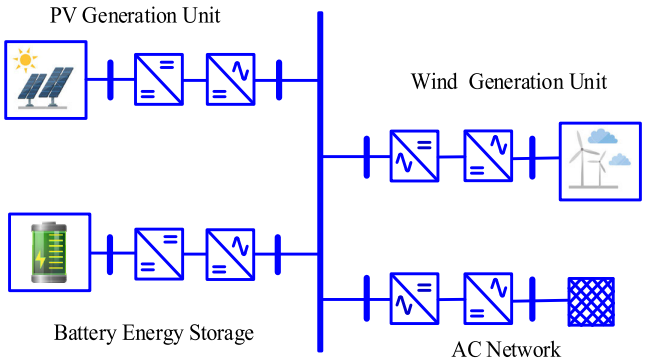

FIGURE 1. A typical architecture of a low-voltage MG with several DG units.

The model of a 3-phase inverter is presented as:

$$L\frac{d}{dt}\left(i_i^J\right) = \mathcal{S}_J V_{dc} - v_{oJn}, \quad J = a, b, c \tag{1}$$

where:

$$\mathcal{S}_a = \begin{cases} 1 & \text{if } \mathcal{S}_1 = \text{ON} \quad \mathcal{S}_4 = \text{OFF} \\ 0 & \text{if } \mathcal{S}_1 = \text{OFF} \quad \mathcal{S}_4 = \text{ON} \end{cases}$$
$$\mathcal{S}_b = \begin{cases} 1 & \text{if } \mathcal{S}_2 = \text{ON} \quad \mathcal{S}_5 = \text{OFF} \\ 0 & \text{if } \mathcal{S}_2 = \text{OFF} \quad \mathcal{S}_5 = \text{ON} \end{cases}$$
$$\mathcal{S}_c = \begin{cases} 1 & \text{if } \mathcal{S} = \text{ON} \quad \mathcal{S}_6 = \text{OFF} \\ 0 & \text{if } \mathcal{S}_3 = \text{OFF} \quad \mathcal{S}_6 = \text{ON} \end{cases} \tag{2}$$

where V_{dc} denotes the dc-link voltage; v_{oan}, v_{obn} and v_{ocn} defines the phase to neutral voltages after filtering, and i_i^a, i_i^b and i_i^c display the phase currents through filter inductor L.

Inverter output voltage vector is displayed in Figure 1 and is defined as bellow:

$$v_i = \frac{2}{3}\left(v_{an} + a v_{bn} + a^2 v_{cn}\right) \tag{3}$$

Assuming all the possible combinations of the gating signals, namely $\mathcal{S}_a$, $\mathcal{S}_b$ and $\mathcal{S}_c$, eight switching modes and as a result, eight voltage vectors have been retrieved. As $v_0 = v_7$, there are just seven different voltage vectors as expressed in Figure 2. Based on KVL:

$$Ri_i^J + L\frac{di_i^J}{dt} = v_i^J(t) - v_o^J(t), \quad J = a, b, c \tag{4}$$

Also, KCL states:

$$C\frac{dv_o^J}{dt} = i_i^J - i_o^J = i_c^J, \quad J = a, b, c \tag{5}$$

State-space representation of each phase is retrieved as:

$$\dot{x}_J(t) = Ax_J(t) + Bv_i^J(t) + Ci_o^J(t), \quad J = a, b, c \tag{6}$$

In which $x_J(t) = \begin{bmatrix} i_i^J(t) \\ v_o^J(t) \end{bmatrix}$ is the state vector.

Also $v_i^J(t)$ defines control command and $i_o^J(t)$ denotes disturbance input and:

$$A = \begin{bmatrix} -\frac{R}{L} & -\frac{1}{L} \\ \frac{1}{C} & 0 \end{bmatrix}, \quad B = \begin{bmatrix} \frac{1}{L} \\ 0 \end{bmatrix}, \quad D = \begin{bmatrix} 0 \\ \frac{1}{C} \end{bmatrix} \tag{7}$$

Eq. (6) is discretized to use in the controller design, therefore:

$$x_J^\alpha[k+1] = A_\alpha x_J^\alpha[k] + B_\alpha v_i[k] + D_\alpha i_o[k]; \; J = a, b, c \tag{8}$$

where: $x_J^\alpha[k] = \begin{bmatrix} i_i^J[k] \\ v_g^J[k] \end{bmatrix}$.

$$A_\alpha = e^{AT_s}, \quad B_\alpha = \int_0^{T_s} e^{A\tau} B d\tau,$$
$$D_\alpha = \int_0^{T_s} e^{A\tau} \Gamma d\tau$$

Also, T_s defines the sampling period.

B. PROBLEM FORMULATION

In this part, we present the problem formulation. Hence, a discrete-time polytopic LPV system with disturbance should be considered, where their system matrices should be related to the functions of a parameter vector ρ_κ as follows:

$$x_{\kappa+1} = A(\rho_\kappa) x_\kappa + B(\rho_\kappa) u_\kappa + D(\rho_\kappa) \omega_\kappa;$$
$$z_\kappa = \begin{bmatrix} C(\rho_\kappa) x_\kappa \\ R(\rho_\kappa) u_\kappa \end{bmatrix} \tag{9}$$

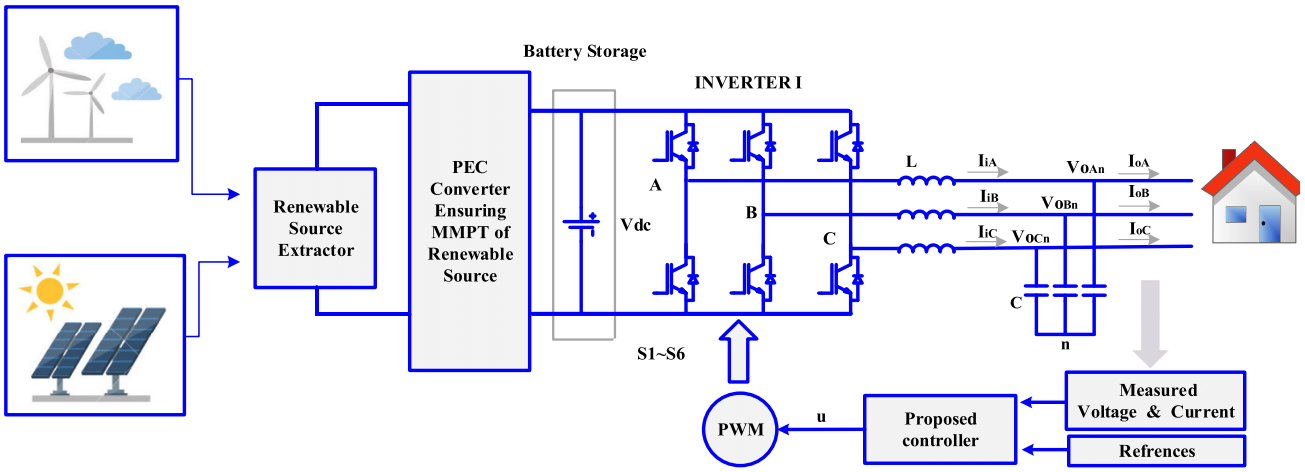

FIGURE 2. A typical structure of a 3-phase low-voltage MG with 2 DG units.

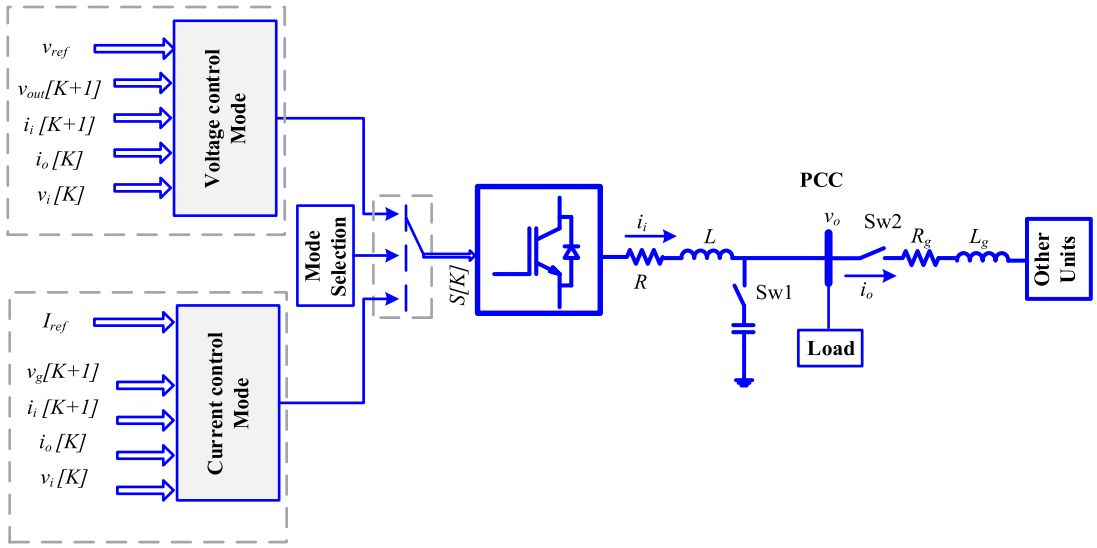

FIGURE 3. Schematic diagram of a typical voltage source inverter by the inverter, output filter, and loads with mode selection of the controller.

With $x \in R^n$ providing the state vector, $u \in R^m$ represents the control input vector, $z \in R^\rho$ is the control output vector, $\omega \in R^{n_\omega}$ gives the disturbance; also:

$$\left[A(\rho_\kappa) \quad B(\rho_\kappa) \quad D(\rho_\kappa) \quad C(\rho_\kappa) \quad R(\rho_\kappa) \right] = \sum_{i=1}^{r} \left[\rho_{\kappa,i} \quad A_i \quad B_i \quad D_i \quad C_i \quad R_i \right].$$

The parameter vector of $p_\kappa \in R^r$ depends on the unit simplex where: $\mathfrak{p} = \left\{ \sum_{i=1}^{r} \rho_i = 1, 0 \le \rho_i \le 1 \right\}$.

The matrices of LPV system change inside a corresponding polytope Ω whose vertices include r local system matrices $\Omega = co\{(A_i, B_i, D_i, C_i, R_i)\}$ where co represents the convex hull.

Lemma 1: It should be supposed that matrices $M \in R^{n\times n}$ and $\mathcal{N} \in R^{m\times n}$ are two positive semidefinite matrices $P \in R^{m\times m}$ and $\mathcal{Q} \in R^{n\times n}$ so that

$$M^T PM - \mathcal{Q} < 0,\ \mathcal{N}^T P\mathcal{N} - \mathcal{Q} < 0$$

Then:

$$M^T P\mathcal{N} + \mathcal{N}^T PM - 2\mathcal{Q} < O$$

Proof:

$$(M-\mathcal{N})^T P(M-\mathcal{N}) = M^T PM + \mathcal{N}^T P\mathcal{N} - M^T P\mathcal{N} - \mathcal{N}^T PM \ge 0$$

$$M^T P\mathcal{N} + \mathcal{N}^T PM - 2\mathcal{Q} \le -M^T PM - \mathcal{N}^T P\mathcal{N} - 2\mathcal{Q} < 0$$

Lemma 2: It should be supposed that matrices $M_i \in R^{m\times n}, i \in \mathcal{N}_r^+$ and are two positive semidefinite matrices $P \in R^{m\times m}$ and $P \in R^{m\times m}$ have been given. The following matrix inequality will be:

$$\left(\sum_{i=1}^{r} \rho_i M_i \right)^T P \left(\sum_{i=1}^{r} \rho_i M_i \right) - \mathcal{Q} < 0 \qquad (10)$$

When $\rho_i > 0$ and $\sum_{i=1}^{r} \rho_i = 1$ if:

$$M_i^T P M_i - \Omega < 0 \tag{11}$$

Proof:

$$\begin{aligned}
&\left(\sum_{i=1}^{r} \rho_i M_i\right)^T P \left(\sum_{i=1}^{r} \rho_i M_i\right) - \Omega \\
&= \sum_{i=1}^{r} \rho_i^2 M_i^T P M_i + \sum_{i=1}^{r} \rho_i^2 M_i^T P M_i \\
&\quad + \sum_{i=1}^{r} \sum_{j=1, j\neq i}^{r} \rho_i \rho_j M_i^T P M_j - \Omega \\
&= \sum_{i=1}^{r} \rho_i^2 \left(M_i^T P M_i - \Omega\right) + \sum_{i=1}^{r} \sum_{j=1, j\neq i}^{r} \rho_i \rho_j \left(M_i^T P M_j - \Omega\right)
\end{aligned}$$

By applying lemma1, it can be seen that equation (10) holds if equation (11) holds.

In the following equations, the problem of system input constraints and measurable modes is considered:

$$|L_l x| \geq f_l, \quad f_l > 0 \quad l = 1, \ldots, n \tag{12}$$

$$|u_l| \geq d_l, \quad d_l > 0 \quad l = 1, \ldots, n \tag{13}$$

In equations (12) and (13): L gives a matrix with L_l as the *lth* line, f_l represents the *lth* element of vector f, u_l is the *lth* element of control input u, and d_l divides the *lth* element of vector d. For the system in equation (9) with constraints equations (12) and (13), the objective is to design a gain-scheduled state feedback control law as follows:

$$u_{\kappa+l|\kappa} = \tilde{F}_{\kappa+l|\kappa} x_{\kappa+l|\kappa} = \sum_{j=1}^{r} \rho_{\kappa+l|\kappa,j} F_{\kappa,j} x_{\kappa+l|\kappa}, \quad i < j, \; l \geq 0 \tag{14}$$

The disturbance will be bounded as:

$$\sum_{\kappa=0}^{\infty} \omega_{\kappa|\kappa}^T \omega_{\kappa|\kappa} \leq \bar{\omega}, \omega_{\kappa|\kappa} \in \pi_q := \left\{\omega | \omega^T q^{-1} \omega \leq 1\right\} \tag{15}$$

In the equation (15), $\bar{\omega} > 0$ and q are known. Hence, the following efficiency requirements are satisfied and divided into two following sections:

1. H_∞ efficiency requirements: under the zero-initial situation, the controlled output $z_{\kappa|\kappa}$ is satisfied as follows:

$$\sum_{\kappa=0}^{\infty} z_{\kappa|\kappa}^T z_{\kappa|\kappa} \leq \varphi^2 \sum_{\kappa=0}^{\infty} \omega_{\kappa|\kappa}^T \omega_{\kappa|\kappa} \quad \text{and} \quad \varphi > 0, \quad \text{scalar} \tag{16}$$

2. H_2 efficiency requirements: the controlled output $z_{\kappa|\kappa}$ is satisfied as follows:

$$\sum_{\kappa=0}^{\infty} z_{\kappa|\kappa}^T z_{\kappa|\kappa} \leq \partial \tag{17}$$

C. GAIN-SCHEDULED CONTROL LAW DESIGN

By rewriting the closed-loop system equation (9) based on the control law equation (14), we will have equation (18) as follows:

$$x_{\kappa+l+1|\kappa} = \left(\sum_{i=1}^{r} \sum_{j=1}^{r} \rho_{\kappa+l|\kappa,i} \rho_{\kappa+l|\kappa,j} \left((A_i + B_i F_j) x_{\kappa+l|\kappa} + (D_i) \omega_{\kappa+l|\kappa}\right)\right) \tag{18}$$

With considering the Lyapunov function in the form $v\left(x_{\kappa+l|\kappa}\right) = x_{\kappa+l|\kappa}^T P_l x_{\kappa+l|\kappa}$ that is multistep P:

$$P_l > 0 \, (l = 0, \ldots, \mathcal{N} - 1) \text{ when } i \geq \mathcal{N} - 1, \; P_l = P_{\mathcal{N}-1}$$

And by assuming $\omega_{\kappa+l|\kappa} = 0$, equation (18) will be converted into:

$$x_{\kappa+l+1|\kappa} = \left(\sum_{i=1}^{r} \sum_{j=1}^{r} \rho_{\kappa+l|\kappa,i} \rho_{\kappa+l|\kappa,j} \left(A_i + B_i F_j\right) x_{\kappa+l|\kappa}\right) \tag{19}$$

By using materials provided in the paper [26], to decrease the conservatism, the state space equation (18) can be presented as follows:

$$\begin{aligned}
x_{\kappa+l+1|\kappa} &= \left(\sum_{i=1}^{r} \rho_{\kappa+l|\kappa,i}^2 \tilde{\mathrm{A}}_{i,i} \right. \\
&\quad \left. + \sum_{i=1}^{r} \sum_{j<i}^{r} 2 \rho_{\kappa+l|\kappa,i} \rho_{\kappa+l|\kappa,j} \left(\frac{\tilde{\mathrm{A}}_{i,j} + \tilde{\mathrm{A}}_{j,i}}{2}\right)\right) x_{\kappa+l|\kappa} \\
\tilde{\mathrm{A}}_{i,j} &= A_i + B_i F_{\kappa,j}
\end{aligned} \tag{20}$$

Then we have, (21) and (22), as shown at the bottom of the next page.

$$\begin{bmatrix} X_{11} & X_{12} & \cdots & X_{1r} \\ X_{12} & X_{22} & \cdots & X_{2r} \\ \vdots & \vdots & \ddots & \vdots \\ X_{1r} & X_{2r} & \cdots & X_{rr} \end{bmatrix} > 0 \tag{23}$$

Thus, if equation (23) holds, ΔV is negative definite, and therefore LPV system of equation (19) will be stable. With considering $\omega_{\kappa+l|\kappa} \neq 0$, (24) and (25), as shown at the bottom of page 7. Then:

$$\beta_{ii} = \tilde{\mathrm{A}}_{i,i}, \quad \overline{\overline{C}}_{ii} = \tilde{C}_{i,i}, \quad \overline{\overline{D}}_{ii} = D_i, \quad \beta_{ij} = \frac{\tilde{\mathrm{A}}_{i,j} + \tilde{\mathrm{A}}_{j,i}}{2}^T,$$

$$\overline{\overline{C}}_{ij} = \frac{C_{i,j} + C_{j,i}}{2}^T, \quad \overline{\overline{D}}_{ij} = \frac{D_i + D_j}{2}, \quad \hat{P}_l = \begin{bmatrix} P_l & 0 \\ 0 & \varphi^2 \end{bmatrix}$$

$$\bar{P}_{l+1} = \begin{bmatrix} P_{l+1} & 0 \\ 0 & I \end{bmatrix}, \quad \xi_{i,i} = \begin{bmatrix} \beta_{i,i}^T & \overline{\overline{C}}_{i,i}^T \\ \overline{\overline{D}}_{i,i}^T & 0 \end{bmatrix},$$

$$\xi_{i,j} = \begin{bmatrix} \beta_{i,j}^T & \overline{\overline{C}}_{i,j}^T \\ \overline{\overline{D}}_{i,j}^T & 0 \end{bmatrix}$$

Lemma 3: By considering the LPV system the equation (9), with disturbance equation (15), the control law that guarantees the efficiency requirements 1 and 2, is given by $F_l = Y_l \mathcal{Q}_l$ if there exist $Y_l \in R^{m\times n}$ and $\mathcal{Q}_l \in R^{n\times n}$ satisfy the following situation:

$$\begin{bmatrix} 1 & * & * \\ \varphi^2\bar{\omega} & \partial\varphi^2\bar{\omega} & * \\ x_{\kappa|\kappa} & 0 & \mathcal{Q}_0 \end{bmatrix} \geq 0 \tag{26}$$

$$\begin{bmatrix} -\mathcal{Q}_l + \bar{X}_{ii}^{(11)} & \bar{X}_{ii}^{(12)} & * & * & * \\ \bar{X}_{ii}^{(21)} & -\varphi^2\partial I + \bar{X}_{ii}^{(22)} & * & * & * \\ A_i\mathcal{Q}_l + B_iY_l & \partial D_i & -\mathcal{Q}_{l+1} & * & * \\ C_i\mathcal{Q}_l & 0 & 0 & -\partial I & * \\ R_iY_l & 0 & 0 & 0 & -\partial I \end{bmatrix} \leq 0 \tag{27}$$

$$\begin{bmatrix} -4\mathcal{Q}_l + \bar{X}_{ij}^{(11)} & \bar{X}_{ij}^{(12)} & * & * & * \\ \bar{X}_{ij}^{(21)} & -4\partial\varphi^2 + \bar{X}_{ij}^{(22)} & * & * & * \\ M_{31} & M_{32} & -\mathcal{Q}_{l+1} & * & * \\ M_{41} & 0 & 0 & -\partial I & * \\ M_{51} & 0 & 0 & 0 & -\partial I \end{bmatrix} \leq 0$$

$$\begin{aligned} M_{31} &= A_i\mathcal{Q}_l + B_iY_l + A_j\mathcal{Q}_l + B_jY_l \\ M_{41} &= C_i\mathcal{Q}_l + C_j\mathcal{Q}_l \\ M_{51} &= R_iY_l + R_jY_l \\ M_{32} &= \partial D_i + \partial D_j \end{aligned} \tag{28}$$

Proof: In equation (9), if M_κ in the equation (25) becomes negative as the disturbance is satisfied in the equation (15), the disturbance will reduce to zero, and then $M_\kappa \leq 0$ implies that $\Delta V(\kappa + l|\kappa) < 0$ after some time instant. Thus, $V(\kappa + l|\kappa)$ goes to zero when $1 = \infty$. As a result, by summing up of both sides of the equation (2)5 from $\kappa = 0$ to $\kappa \to \infty$, it yields; consequently, it will be retrieved as:

$$\begin{aligned} &-x_{\kappa|\kappa}^T P_0 x_{\kappa|\kappa} \\ &= \sum_{l=0}^{\infty}\left(\varphi^2\omega_{\kappa+l|\kappa}^T\omega_{\kappa+l|\kappa} - z_{\kappa+l|\kappa}^T z_{\kappa+l|\kappa}\right) \\ &\quad + \sum_{l=0}^{\infty}\left[x_{\kappa+l|\kappa}{}^T \;\; \omega_{\kappa+l|\kappa}{}^T\right] M_\kappa \left[x_{\kappa+l|\kappa}{}^T \;\; \omega_{\kappa+l|\kappa}{}^T\right]^T \end{aligned} \tag{29}$$

Equation (29) can be transformed into:

$$\begin{aligned} &\sum_{l=0}^{\infty} z_{\kappa+l|\kappa}^T z_{\kappa+l} \\ &\quad = x_{\kappa|\kappa}^T P_0 x_{\kappa|\kappa} + \sum_{l=0}^{\infty}\varphi^2\omega_{\kappa+l|\kappa}^T\omega_{\kappa+l|\kappa} \\ &\quad\quad + \sum_{l=0}^{\infty}\left[x_{\kappa+l|\kappa}{}^T \;\; \omega_{\kappa+l|\kappa}{}^T\right] M_\kappa \left[x_{\kappa+l|\kappa}{}^T \;\; \omega_{\kappa+l|\kappa}{}^T\right]^T \end{aligned} \tag{30}$$

From the efficiency requirements 1 and 2, when $x_{\kappa|\kappa} = 0$, it will be under the zero-initial condition, the requirement equation (16) will be equal to:

$$\begin{aligned} \sum_{l=0}^{\infty} z_{\kappa+l|\kappa}^T z_{\kappa+l|\kappa} \leq \sum_{l=0}^{\infty}\varphi^2\omega_{\kappa+l|\kappa}^T\omega_{\kappa+l|\kappa} \to \sum_{l=0}^{\infty} z_{\kappa+l|\kappa}^T z_{\kappa+l|\kappa} \\ -\varphi^2\sum_{l=0}^{\infty}\omega_{\kappa+l|\kappa}^T\omega_{\kappa+l|\kappa} \leq 0 \end{aligned} \tag{31}$$

$$\begin{aligned} \Delta V|(19) &= \Delta V(\kappa + l|\kappa) = V(\kappa + l + 1|\kappa) - V(\kappa + l|\kappa) = \left\|A\left(\rho_{\kappa+l|\kappa}\right)x_{\kappa+l|\kappa} + B\left(\rho_{\kappa+l|\kappa}\right)u_{\kappa+l|\kappa}\right\|_{P_{l+1}}^2 - \left\|x_{\kappa+l|\kappa}\right\|_{P_l}^2 \\ &= \mathrm{x}_{\kappa+l|\kappa}{}^{\mathrm{T}}\left[\begin{array}{c}\left(\sum_{\mathrm{i}=1}^{\mathrm{r}}\rho_{\kappa+1|\kappa,\mathrm{i}}^2\tilde{\mathrm{A}}_{\mathrm{i,i}} + \sum_{\mathrm{i}=1}^{\mathrm{r}}\sum_{\mathrm{j}<\mathrm{i}}^{\mathrm{r}}2\rho_{\kappa+l|\kappa,i}\rho_{\kappa+1|\kappa,\mathrm{j}}\left(\frac{\tilde{\mathrm{A}}_{\mathrm{i,j}} + \tilde{\mathrm{A}}_{\mathrm{j,i}}}{2}\right)\right)^{\mathrm{T}}\mathrm{P}_{\mathrm{l}+1} \\ \left(\sum_{\mathrm{i}=1}^{\mathrm{r}}\rho_{\kappa+1|\kappa,\mathrm{i}}^2\tilde{\mathrm{A}}_{\mathrm{i,i}} + \sum_{\mathrm{i}=1}^{\mathrm{r}}\sum_{\mathrm{j}<\mathrm{i}}^{\mathrm{r}}2\rho_{\kappa+l|\kappa,i}\rho_{\kappa+1|\kappa,\mathrm{j}}\left(\frac{\tilde{\mathrm{A}}_{\mathrm{i,j}} + \tilde{\mathrm{A}}_{\mathrm{j,i}}}{2}\right)\right)\end{array}\right]\ldots\ldots x_{\kappa+l|\kappa} \\ &\quad - x_{\kappa+l|\kappa}{}^T(P_l)\,x_{\kappa+l|\kappa} \end{aligned} \tag{21}$$

$$\begin{aligned} \Delta V|(19) &= x_{\kappa+l|\kappa}{}^T\left[\sum_{i=1}^{r}\rho_{\kappa+l|\kappa,i}^2\left(\tilde{\mathrm{A}}_{i,i}{}^T P_{l+1}\tilde{\mathrm{A}}_{i,i} - P_l\right)\right]x_{\kappa+l|\kappa} \\ &\quad + x_{\kappa+l|\kappa}{}^T\left[\sum_{i=1}^{r}\sum_{j<i}^{r}2\rho_{\kappa+l|\kappa,i}\rho_{\kappa+l|\kappa,j}\left(\left(\frac{\tilde{\mathrm{A}}_{i,j} + \tilde{\mathrm{A}}_{j,i}}{2}\right)^T P_{l+1}\left(\frac{\tilde{\mathrm{A}}_{i,j} + \tilde{\mathrm{A}}_{j,i}}{2}\right) - P_l\right)\right]x_{\kappa+l|\kappa} \\ &\leq x_{\kappa+l|\kappa}{}^T\left[-\sum_{i=1}^{r}\rho_{\kappa+l|\kappa,i}^2 X_{i,i} - \sum_{i=1}^{r}\sum_{j<i}^{r}2\rho_{\kappa+l|\kappa,i}\rho_{\kappa+l|\kappa,j}X_{i,j}\right]x_{\kappa+l|\kappa} \\ &= -\begin{bmatrix}\rho_{\kappa+l|\kappa,1}x_{\kappa+l|\kappa} \\ \rho_{\kappa+l|\kappa,2}x_{\kappa+l|\kappa} \\ \vdots \\ \rho_{\kappa+l|\kappa,r}x_{\kappa+l|\kappa}\end{bmatrix}^T\begin{bmatrix}X_{11} & X_{12} & \cdots & X_{1r} \\ X_{12} & X_{22} & \cdots & X_{2r} \\ \vdots & \vdots & \ddots & \vdots \\ X_{1r} & X_{2r} & \cdots & X_{rr}\end{bmatrix}\begin{bmatrix}\rho_{\kappa+l|\kappa,1}x_{\kappa+l|\kappa} \\ \rho_{\kappa+l|\kappa,2}x_{\kappa+l|\kappa} \\ \vdots \\ \rho_{\kappa+l|\kappa,r}x_{\kappa+l|\kappa}\end{bmatrix} \end{aligned} \tag{22}$$

By considering the equation (30), if $M_\kappa \leq 0$ holds, the equation (16) is satisfied which in turn the requirement on $H\infty$ efficiency will be satisfied.

Under the situation that $M_\kappa \leq 0$, the requirement of equation 17 is satisfied if:

$$\sum_{l=0}^{\infty} z_{\kappa+l|\kappa}^T z_{\kappa+l|\kappa} \leq x_{\kappa|\kappa}^T P_0 x_{\kappa|\kappa} + \varphi^2\bar{\omega} \leq \partial \rightarrow \partial - x_{\kappa|\kappa}^T P_0 x_{\kappa|\kappa} + \varphi^2\bar{\omega} \geq 0 \quad (32)$$

By multiplying the sides in ∂^{-1}:

$$1 - x_{\kappa|\kappa}^T P_0 \partial^{-1} x_{\kappa|\kappa} + \varphi^2\bar{\omega}\partial^{-1}\varphi^2\bar{\omega}^{-1}\varphi^2\bar{\omega} \geq 0$$

By Schur complement:

$$\begin{bmatrix} 1 & * & * \\ \varphi^2\bar{\omega} & \partial\varphi^2\bar{\omega} & * \\ x_{\kappa|\kappa} & 0 & \mathcal{Q}_0 \end{bmatrix} \geq 0$$

According to the above-mentioned assessment, it can be concluded that for the design aim, $M_\kappa \leq 0$, is a vital issue, that is, (33) and (34), as shown at the bottom of the next page.

According to equations (33) and (34) and also lemma 2, (35), as shown at the bottom of the next page.

$$\begin{aligned}
\Delta V|23 = \Delta V(\kappa+l|\kappa) &= V(\kappa+l+1|\kappa) - V(\kappa+l|\kappa) = \left\| A\left(\rho_{\kappa+l|\kappa}\right) x_{\kappa+l|\kappa} \right. \\
&\left. + B\left(\rho_{\kappa+l|\kappa}\right) u_{\kappa+l|\kappa} + D\left(\rho_{\kappa+l|\kappa}\right) \omega_{\kappa+l|\kappa} \right\|_{P_{l+1}}^2 - \left\| x_{\kappa+l|\kappa} \right\|_{P_l}^2 \\
&= x_{\kappa+l|\kappa}^T \left[\begin{array}{c} \left(\sum_{i=1}^{r} \rho_{\kappa+l|\kappa,i}^2 \tilde{\mathrm{A}}_{i,i} + 2\sum_{i=1}^{r}\sum_{j<i}^{r} \rho_{\kappa+l|\kappa,i}\rho_{\kappa+l|\kappa,j} \left(\frac{\tilde{\mathrm{A}}_{i,j} + \tilde{\mathrm{A}}_{j,i}}{2} \right) \right)^T P_{l+1} \\ \left(\sum_{i=1}^{r} \rho_{\kappa+l|\kappa,i}^2 \tilde{\mathrm{A}}_{i,i} + 2\sum_{i=1}^{r}\sum_{j<i}^{r} \rho_{\kappa+l|\kappa,i}\rho_{\kappa+l|\kappa,j} \left(\frac{\tilde{\mathrm{A}}_{i,j} + \tilde{\mathrm{A}}_{j,i}}{2} \right) \right) \end{array} \right] x_{k+l|k} \\
&+ \omega_{\kappa+l|\kappa}^T \left[\begin{array}{c} \left(\sum_{i=1}^{r} \rho_{\kappa+l|\kappa,i}^2 \tilde{D}_{i,i} + 2\sum_{i=1}^{r}\sum_{j<i}^{r} \rho_{\kappa+l|\kappa,i}\rho_{\kappa+l|\kappa,j} \left(\frac{\tilde{D}_{i,j} + \tilde{D}_{j,i}}{2} \right) \right)^T P_{l+1} \\ \left(\sum_{i=1}^{r} \rho_{\kappa+l|\kappa,i}^2 \tilde{D}_{i,i} + 2\sum_{i=1}^{r}\sum_{j<i}^{r} \rho_{\kappa+l|\kappa,i}\rho_{\kappa+l|\kappa,j} \left(\frac{\tilde{D}_{i,j} + \tilde{D}_{j,i}}{2} \right) \right) \end{array} \right] w_{k+l|k} \\
&+ 2\omega_{\kappa+l|\kappa}^T \left[\begin{array}{c} \left(\sum_{i=1}^{r} \rho_{\kappa+l|\kappa,i}^2 \tilde{D}_{i,i} + 2\sum_{i=1}^{r}\sum_{j<i}^{r} \rho_{\kappa+l|\kappa,i}\rho_{\kappa+l|\kappa,j} \left(\frac{\tilde{D}_{i,j} + \tilde{D}_{j,i}}{2} \right) \right)^T P_{l+1} \\ \left(\sum_{i=1}^{r} \rho_{\kappa+l|\kappa,i}^2 \tilde{\mathrm{A}}_{i,i} + 2\sum_{i=1}^{r}\sum_{j<i}^{r} \rho_{\kappa+l|\kappa,i}\rho_{\kappa+l|\kappa,j} \left(\frac{\tilde{\mathrm{A}}_{i,j} + \tilde{\mathrm{A}}_{j,i}}{2} \right) \right) \end{array} \right] x_{\kappa+l|\kappa} \\
&- x_{\kappa+l|\kappa}^T \left[\begin{array}{c} \left(\sum_{i=1}^{r} \tilde{C}_{i,i}\rho_{\kappa+l|\kappa,i}^2 + 2\sum_{i=1}^{r}\sum_{j<i}^{r} \rho_{\kappa+l|\kappa,i}\rho_{\kappa+l|\kappa,j} \left(\frac{\tilde{C}_{i,j} + \tilde{C}_{j,i}}{2} \right) \right) \times \\ \left(\sum_{i=1}^{r} \tilde{C}_{i,i}\rho_{\kappa+l|\kappa,i}^2 + 2\sum_{i=1}^{r}\sum_{j<i}^{r} \rho_{\kappa+l|\kappa,i}\rho_{\kappa+l|\kappa,j} \left(\frac{\tilde{C}_{i,j} + \tilde{C}_{j,i}}{2} \right) \right) \end{array} \right] x_{\kappa+l|\kappa} \\
&+ {x_{\kappa+l|\kappa}}^T \left[\begin{array}{c} \left(\sum_{i=1}^{r} \tilde{C}_{i,i}\rho_{\kappa+l|\kappa,i}^2 + 2\sum_{i=1}^{r}\sum_{j<i}^{r} \rho_{\kappa+l|\kappa,i}\rho_{\kappa+l|\kappa,j} \left(\frac{\tilde{C}_{i,j} + \tilde{C}_{j,i}}{2} \right) \right) \times \\ \left(\sum_{i=1}^{r} \tilde{C}_{i,i}\rho_{\kappa+l|\kappa,i}^2 + 2\sum_{i=1}^{r}\sum_{j<i}^{r} \rho_{\kappa+l|\kappa,i}\rho_{\kappa+l|\kappa,j} \left(\frac{\tilde{C}_{i,j} + \tilde{C}_{j,i}}{2} \right) \right) \end{array} \right] x_{\kappa+l|\kappa} \\
&+ \varphi^2\omega_{\kappa+l|\kappa}^T\omega_{\kappa+l|\kappa} - \varphi^2\omega_{\kappa+l|\kappa}^T\omega_{\kappa+l|\kappa} - {x_{\kappa+l|\kappa}}^T (P_l) x_{\kappa+l|\kappa} \qquad (24)
\end{aligned}$$

$$\Delta V(\kappa+l|\kappa) = \left[{x_{\kappa+l|\kappa}}^T \quad {\omega_{\kappa+l|\kappa}}^T \right] M_\kappa \left[{x_{\kappa+l|\kappa}}^T \quad {\omega_{\kappa+l|\kappa}}^T \right]^T + \varphi^2\omega_{\kappa+l|\kappa}^T\omega_{\kappa+l} - z_{\kappa+l|\kappa}^T z_{\kappa+l|\kappa}$$

$$M_\kappa = \left[\sum_{i=1}^{r} \rho_{\kappa+l|\kappa,i}^2 \xi_{i,i}^T \bar{P}_{l+1} \xi_{i,i} + 2\sum_{i=1}^{r}\sum_{j<i}^{r} \rho_{\kappa+l|\kappa,i}\rho_{\kappa+l|\kappa,j} \left(\frac{\xi_{i,j} + \xi_{j,i}}{2} \right)^T \bar{P}_{l+1} \left(\frac{\xi_{i,j} + \xi_{j,i}}{2} \right) \right] - \hat{P}_l \qquad (25)$$

By applying Schur complement, equation (35) is converted into its LMI form as follows:

$$\begin{bmatrix} -P_l + X_{iil}^{(11)} & X_{iil}^{(12)} & * & * & * \\ X_{iil}^{(21)} & -\varphi^2 I + X_{iil}^{(22)} & * & * & * \\ A_i + B_i F_{l,i} & D_i & -P_{l+1} & * & * \\ C_i & 0 & 0 & -I & * \\ R_i F_l & 0 & 0 & 0 & -I \end{bmatrix} \leq 0$$

$$\begin{bmatrix} -4P_l + X_{ijl}^{(11)} & X_{ijl}^{(12)} & * & * & * \\ X_{ijl}^{(21)} & -4\varphi^2 + X_{ijl}^{(22)} & * & * & * \\ M_{31} & M_{32} & -P_{l+1} & * & * \\ M_{41} & 0 & 0 & -I & * \\ M_{51} & 0 & 0 & 0 & -I \end{bmatrix} \leq 0$$

$$M_{31} = A_i + B_i F_{l,j} + A_j + B_j F_{l,i}$$

$$\begin{aligned} M_{41} &= C_i + C_j \\ M_{51} &= R_i F_l, j + R_j F_l, j \\ M_{32} &= D_i + D_j \end{aligned} \tag{36}$$

Pre- and post-multiplying equation (36) considering $\left\{\partial^{1/2} P_l^{-1},\ \partial^{1/2} I,\ \partial^{1/2} I,\ \partial^{1/2} I,\ \partial^{1/2} I\right\}$ is presented in equation (37), as shown at the bottom of the next page.

Setting:

$$\begin{aligned} \mathcal{Q}_l &= \partial P_l^{-1}, F_l = Y_l \mathcal{Q}_l^{-1} \\ \bar{X}_{ii}^{(11)} &= \partial P_l^{-1} X_{iil}^{(11)} P_l^{-1} \\ \bar{X}_{ii}^{(12)} &= \partial P_l^{-1} X_{ijl}^{(12)} \\ \bar{X}_{ii}^{(22)} &= \partial X_{iil}^{(22)} \end{aligned}$$

$$\begin{aligned} \zeta_{\kappa+l|\kappa} &= \begin{bmatrix} x_{\kappa+l|\kappa}^T & \omega_{\kappa+l|\kappa}^T \end{bmatrix}^T \\ M_\kappa &= \zeta_{\kappa+l|\kappa}^T \left[\sum_{i=1}^{r} \rho_{\kappa+l|\kappa,i}^2 \left(\xi_{i,i}^T \bar{P}_{l+1} \xi_{i,i} - \hat{P}_l \right) \right] \zeta_{\kappa+l|\kappa} \\ &\quad + 2\zeta_{\kappa+l|\kappa}{}^T \left[\sum_{i=1}^{r} \sum_{j<i}^{r} \rho_{\kappa+l|\kappa,i} \rho_{\kappa+l|\kappa,j} \left(\left(\frac{\xi_{i,j} + \xi_{j,i}}{2} \right)^T \bar{P}_{l+1} \left(\frac{\xi_{i,j} + \xi_{j,i}}{2} \right) - \hat{P}_l \right) \right] \zeta_{\kappa+l|\kappa} \\ &\leq -\left(\zeta_{\kappa+l|\kappa}{}^T \left[\sum_{i=1}^{r} \rho_{\kappa+l|\kappa,i}^2 X_{iil} \right] \zeta_{\kappa+l|\kappa} + 2\zeta_{\kappa+l|\kappa}{}^T \left[\sum_{i=1}^{r} \sum_{j<i}^{r} \rho_{\kappa+l|\kappa,i} \rho_{\kappa+l|\kappa,j} X_{ijl} \right] \zeta_{\kappa+l|\kappa} \right) \\ &= -\begin{bmatrix} \rho_{\kappa+l|\kappa,1}\zeta_{\kappa+l|\kappa} \\ \rho_{\kappa+l|\kappa,2}\zeta_{\kappa+l|\kappa} \\ \vdots \\ \rho_{\kappa+l|\kappa,r}\zeta_{\kappa+l|\kappa} \end{bmatrix}^T \begin{bmatrix} X_{11l} & X_{12l} & \cdots & X_{1rl} \\ X_{12l} & X_{22l} & \cdots & X_{2rl} \\ \vdots & \vdots & \ddots & \vdots \\ X_{1rl} & X_{2rl} & \cdots & X_{rrl} \end{bmatrix} \begin{bmatrix} \rho_{\kappa+l|\kappa,1}\zeta_{\kappa+l|\kappa} \\ \rho_{\kappa+l|\kappa,2}\zeta_{\kappa+l|\kappa} \\ \vdots \\ \rho_{\kappa+l|\kappa,r}\zeta_{\kappa+l|\kappa} \end{bmatrix} \end{aligned} \tag{33}$$

$$\begin{bmatrix} X_{11l} & X_{12l} & \cdots & X_{1rl} \\ X_{12l} & X_{22l} & \cdots & X_{2rl} \\ \vdots & \vdots & \ddots & \vdots \\ X_{1rl} & X_{2rl} & \cdots & X_{rrl} \end{bmatrix} > 0, \quad X_{iil} = \begin{bmatrix} X_{iil}^{(11)} & X_{iil}^{(21)T} \\ X_{iil}^{(21)} & X_{iil}^{(22)} \end{bmatrix}, \quad X_{ijl} = \begin{bmatrix} X_{ijl}^{(11)} & X_{ijl}^{(21)T} \\ X_{ijl}^{(21)} & X_{ijl}^{(22)} \end{bmatrix}$$

$$\begin{bmatrix} X_{11l}^{(11)} & X_{11l}^{(21)T} & X_{12l}^{(11)} & X_{12l}^{(21)T} & \cdots & X_{1rl}^{(11)} & X_{1rl}^{(21)T} \\ X_{11l}^{(21)} & X_{11l}^{(22)} & X_{12l}^{(21)} & X_{12l}^{(22)} & \cdots & X_{1rl}^{(21)} & X_{1rl}^{(22)} \\ \vdots & \vdots & \vdots & \vdots & \ddots & \vdots & \vdots \\ X_{1rl}^{(11)} & X_{1rl}^{(21)T} & X_{2rl}^{(11)} & X_{2rl}^{(21)T} & \cdots & X_{rrl}^{(11)} & X_{rrl}^{(21)T} \\ X_{1rl}^{(21)} & X_{1rl}^{(22)} & X_{2rl}^{(21)} & X_{2rl}^{(22)} & \cdots & X_{rrl}^{(21)} & X_{rrl}^{(22)} \end{bmatrix} > 0 \tag{34}$$

$$\begin{aligned} &\begin{bmatrix} \tilde{\mathrm{A}}_{i,i}^T & \tilde{C}_{i,i}^T \\ D_i^T & 0 \end{bmatrix} \begin{bmatrix} P_{l+1} & 0 \\ 0 & I \end{bmatrix} \begin{bmatrix} \tilde{\mathrm{A}}_{i,i} & D_i \\ \tilde{C}_{i,i} & 0 \end{bmatrix} - \begin{bmatrix} P_l & 0 \\ 0 & \varphi^2 \end{bmatrix} \\ &\quad \leq -\begin{bmatrix} X_{iil}^{(11)} & X_{iil}^{(12)} \\ X_{iil}^{(21)} & X_{iil}^{(22)} \end{bmatrix} \begin{bmatrix} \left(\tilde{\mathrm{A}}_{i,j} + \tilde{\mathrm{A}}_{j,i}^T \right)^T & \left(C_{i,j} + C_{j,i}^T \right)^T \\ D_i + D_j{}^T & 0 \end{bmatrix} \begin{bmatrix} P_{l+1} & 0 \\ 0 & I \end{bmatrix} \begin{bmatrix} \tilde{\mathrm{A}}_{i,j} + \tilde{\mathrm{A}}_{j,i}^T & D_i + D_j{}^T \\ C_{i,j} + C_{j,i}^T & 0 \end{bmatrix} \\ &\quad -\begin{bmatrix} 4P_l & 0 \\ 0 & 4\varphi^2 \end{bmatrix} \leq -\begin{bmatrix} X_{ijl}^{(11)} & X_{ijl}^{(12)} \\ X_{ijl}^{(21)} & X_{ijl}^{(22)} \end{bmatrix} \end{aligned} \tag{35}$$

$$\begin{aligned}\bar{X}_{ij}^{(11)} &= \partial P_l^{-1} X_{ijl}^{(11)} P_l^{-1}\\ \bar{X}_{ij}^{(12)} &= \partial P_l^{-1} X_{ijl}^{(12)}\\ \bar{X}_{ij}^{(22)} &= \partial X_{ijl}^{(22)}\end{aligned} \tag{38}$$

Consequently, we can define equation (39) as follows:

$$\begin{bmatrix} -Q_l + \bar{X}_{ii}^{(11)} & \bar{X}_{ii}^{(12)} & * & * & * \\ \bar{X}_{ii}^{(21)} & -\varphi^2\partial I + \bar{X}_{ii}^{(22)} & * & * & * \\ A_iQ_l + B_iY_l & \partial D_i & -Q_{l+1} & * & * \\ C_iQ_l & 0 & 0 & -\partial I & * \\ R_iY_l & 0 & 0 & 0 & -\partial I \end{bmatrix} \leq 0$$

$$\begin{bmatrix} -4Q_l + \bar{X}_{ij}^{(11)} & \bar{X}_{ij}^{(12)} & * & * & * \\ \bar{X}_{ij}^{(21)} & -4\partial\varphi^2 + \bar{X}_{ij}^{(22)} & * & * & * \\ M_{31} & M_{32} & -Q_{l+1} & * & * \\ M_{41} & 0 & 0 & -\partial I & * \\ M_{51} & 0 & 0 & 0 & -\partial I \end{bmatrix} \leq 0$$

$$\begin{aligned} M_{31} &= A_i\mathcal{Q}_l + B_iY_l + A_j\mathcal{Q}_l + B_jY_l\\ M_{41} &= C_i\mathcal{Q}_l + C_j\mathcal{Q}_l\\ M_{51} &= R_iY_l + R_jY_l\\ M_{32} &= \partial D_i + \partial D_j \end{aligned} \tag{39}$$

By investigating conditions of the equation (25), it is obvious that equations (26), (27) and (28) cannot guarantee $-z_{\kappa+l|\kappa}^T z_{\kappa+l} + \varphi^2\omega_{\kappa+l|\kappa}^T\omega_{\kappa+l} < 0$ because of the disturbance, which illustrates that the Lyapunov function is not reducing when the disturbance exists. As a result, even if $M_i(\kappa) \leq 0$, $\Delta V < 0$ cannot be guaranteed. Or, even if the current state $x_{\kappa|\kappa}$ belongs to set $\left\{x|x_{\kappa|\kappa}\mathcal{Q}_0^{-1}x_{\kappa|\kappa} \leq 1\right\}$ cannot be guaranteed to belong to $\left\{x|x_{\kappa|\kappa}\mathcal{Q}_l^{-1}x_{\kappa|\kappa} \leq 1\right\}$. The study [26] did not take this issue into account, therefore, it cannot guarantee the recursive feasibility of MPC. Herein, we will give the following lemma to overcome this weakness.

Lemma 4: For systems as given in the equation (9), if equation (25) is satisfied for $x_{\kappa|\kappa}$ and the following inequalities hold, and then, $x_{\kappa+l|\kappa} \in \left\{x|x_{\kappa|\kappa}\mathcal{Q}_l^{-1}x_{\kappa|\kappa} \leq 1\right\}$. In this regard, we will have:

$$\begin{bmatrix} bq^{-1} & * \\ D & \mathcal{Q}_\omega^l \end{bmatrix} \geq 0 \tag{40}$$

$$\begin{bmatrix} \mathcal{Q}_l + \bar{X}_{ii}^{(11)} & \bar{X}_{ii}^{(12)} & * & * & * \\ \bar{X}_{ii}^{(21)} & -\varphi^2\partial I + \bar{X}_{ii}^{(22)} & * & * & * \\ -A_i\mathcal{Q}_l + B_iY_l & \partial D_i & -\zeta_{l+1} & * & * \\ C_i\mathcal{Q}_l & 0 & 0 & -\partial I & * \\ R_iY_l & 0 & 0 & 0 & -\partial I \end{bmatrix} \leq 0$$

$$\begin{bmatrix} -4\mathcal{Q}_l + \bar{X}_{ij}^{(11)} & \bar{X}_{ij}^{(12)} & * & * & * \\ \bar{X}_{ij}^{(21)} & -4\partial\varphi^2 + \bar{X}_{ij}^{(22)} & * & * & * \\ M_{31} & M_{32} & -\zeta_{l+1} & * & * \\ M_{41} & 0 & 0 & -\partial I & * \\ M_{51} & 0 & 0 & 0 & -\partial I \end{bmatrix} \leq 0 \tag{41}$$

$$\begin{aligned} M_{31} &= A_i\mathcal{Q}_l + B_iY_l + A_j\mathcal{Q}_l + B_jY_l\\ M_{41} &= C_i\mathcal{Q}_l + C_j\mathcal{Q}_l\\ M_{51} &= R_iY_l + R_jY_l\\ M_{32} &= \partial D_i + \partial D_j \end{aligned} \tag{42}$$

where $\boldsymbol{\zeta_{l+1}} = (1-b)(\mathcal{Q}_{l+1} - \mathcal{Q}_\omega), l = 0, \ldots, N-1$, $\mathcal{Q}_w$ is a matrix variable and b is a parameter taken into account in advance such that $\mathbf{0} < \boldsymbol{b} < \mathbf{1}$.

Proof: The state at time $\kappa + l + 1$ is $x_{\kappa+l+1|\kappa} = (A_i + B_iF_l)x_{\kappa+l|\kappa} + D_i\omega_{\kappa+l|\kappa}$ according to (1). Denote: $v_{\kappa+l|\kappa} = D_i\omega_{\kappa+l|\kappa}$ and $\tilde{x}_{\kappa+l+1|\kappa} = (A_i + B_iF_l)x_{\kappa+l|\kappa}$.

$$\begin{bmatrix} -\partial P_l^{-1} + \partial P_l^{-1} X_{iil}^{(11)} P_l^{-1} & \partial P_l^{-1} X_{iil}^{(12)} & * & * & * \\ X_{iil}^{(21)}\partial P_l^{-1} & -\partial\varphi^2 I + \partial X_{iil}^{(22)} & * & * & * \\ A_i\partial P_l^{-1} + B_iY_l & \partial D_i & -\partial P_{l+1} & * & * \\ C_i\partial P_l^{-1} & 0 & 0 & -\partial I & * \\ R_iY_l & 0 & 0 & 0 & -\partial I \end{bmatrix} \leq 0$$

$$\begin{bmatrix} -4\partial P_l^{-1} + \partial P_l^{-1} X_{ijl}^{(11)} P_l^{-1} & \partial P_l^{-1} X_{ijl}^{(12)} & * & * & * \\ X_{ijl}^{(21)}\partial P_l^{-1} & -4\partial\varphi^2 + \partial X_{ijl}^{(22)} & * & * & * \\ M_{31} & M_{32} & -\partial P_{l+1} & * & * \\ M_{41} & 0 & 0 & -\partial I & * \\ M_{51} & 0 & 0 & 0 & -\partial I \end{bmatrix} \leq 0$$

$$\begin{aligned} M_{31} &= A_i\partial P_l^{-1} + B_iY_l + A_j\partial P_l^{-1} + B_jY_l\\ M_{41} &= C_i\partial P_l^{-1} + C_j\partial P_l^{-1}\\ M_{51} &= R_iY_l + R_jY_l\\ M_{32} &= \partial D_i + \partial D_j \end{aligned} \tag{37}$$

$x_{\kappa+l+1|\kappa} \in \left\{x | x_{\kappa|\kappa} \mathcal{Q}_{l+1}^{-1} x_{\kappa|\kappa} \leq 1\right\}$ will be guaranteed if the inequality equation (43) is to be considered.

$$\begin{bmatrix} 1 & * \\ x_{\kappa+l+1|\kappa} & \mathcal{Q}_{l+1} \end{bmatrix} \geq 0$$
$$\Leftrightarrow \begin{bmatrix} 1 & * \\ \tilde{x}_{\kappa+l+1|\kappa} + v_{\kappa+l|\kappa} & \mathcal{Q}_{l+1} \end{bmatrix} \geq 0 \quad (43)$$
$$\begin{bmatrix} 1-b & * \\ \tilde{x}_{\kappa+l+1|\kappa} & \mathcal{Q}_{l+1} - \mathcal{Q}_{\omega}^{l} \end{bmatrix} \geq 0 \quad (44)$$
$$\begin{bmatrix} b & * \\ v_{\kappa+l|\kappa} & \mathcal{Q}_{\omega}^{l} \end{bmatrix} \geq 0 \quad (45)$$

where $0 < b < 1$ and $\mathcal{Q}_{\omega}$ represents the matrix variable. Condition equation (15), i.e., $w_{\kappa+l|\kappa} \epsilon \pi_q$, implies that:

$$\begin{bmatrix} 1 & * \\ \omega_{\kappa+l|\kappa} & q \end{bmatrix} \geq 0 \quad (46)$$

And $b \geq \omega_{\kappa+l|\kappa}^{T} b q^{-1} \omega_{\kappa+l|\kappa}$. From equation (45) and (46), it can be observed that equation (45) is guaranteed if the inequality $b \geq \omega_{\kappa+l|\kappa}^{T} b q^{-1} \omega_{\kappa+l|\kappa} \geq \omega_{\kappa+l|\kappa}^{T} D^{T} \mathcal{Q}_{\omega}^{-1} D \omega_{\kappa+l|\kappa}$ holds, which means $b q^{-1} \geq D^{T} \mathcal{Q}_{\omega}^{-1} D$, that is equal to the following condition by applying Schur complement.

$$\begin{bmatrix} b q^{-1} & * \\ D & \mathcal{Q}_{\omega}^{l} \end{bmatrix} \geq 0 \quad (47)$$

where parameter b $(0 < b < 1)$ is a prior chosen parameter. Then since equation (26) holds for $\omega_{\kappa|\kappa}$, and also if:

$$\tilde{x}_{\kappa+l+1|\kappa}^{T} \zeta_{l+1}^{-1} \tilde{x}_{\kappa+l+1|\kappa} \leq x_{\kappa+l|\kappa} \mathcal{Q}_{l}^{-1} x_{\kappa+l|\kappa}$$
$$\text{and } \zeta = (1-b)\left(\mathcal{Q}_{l+1} - \mathcal{Q}_{\omega}\right) \quad (48)$$

It can be guaranteed that $x_{\kappa+l+1|\kappa}$ belongs to set $\left\{x | x_{\kappa|\kappa} \mathcal{Q}_{l+1}^{-1} x_{\kappa|\kappa} \leq 1\right\}$.

The constraints of the system inputs and also measurable states can be presented by:

$$\begin{aligned} \left|L_g x\right| &\leq f_g \text{ and } f_g > 0, \quad (g = 1, \ldots, n) \\ &\rightarrow\rightarrow \begin{bmatrix} O_l & * \\ (L\mathcal{Q}_l)^{T} & \mathcal{Q}_l \end{bmatrix}, \; O_{l,gg} \leq f_l^2 \; (g = 1, \ldots, n) \end{aligned} \quad (49)$$

Proof:

$$\begin{aligned} \left|L_g \mathcal{Q}_l^{\frac{1}{2}} \mathcal{Q}_l^{-\frac{1}{2}} x_{\kappa+l|\kappa}\right| &\leq f_g^2 \\ &\rightarrow \left\|L_g \mathcal{Q}_l^{\frac{1}{2}}\right\|^2 \left\|\mathcal{Q}_l^{-} \frac{1}{2} x_{\kappa+l|\kappa}\right\|^2 \leq f_g^2 \\ &\rightarrow \xrightarrow{\left\|\mathcal{Q}_l^{-\frac{1}{2}} x_{\kappa+l|\kappa}\right\|^2 \leq 1} \left\|L_g \mathcal{Q}_l^{\frac{1}{2}}\right\|^2 \leq f_g^2 \\ &\rightarrow L_g \mathcal{Q}_l^{\frac{1}{2}} \mathcal{Q}_l^{\frac{1}{2}} L_g \leq f_g^2 \\ &\rightarrow L_g \mathcal{Q}_l \mathcal{Q}_l^{-1} \mathcal{Q}_l L_g \leq f_g^2 \end{aligned}$$

$$\begin{aligned} f_g^2 - L\mathcal{Q}_l \mathcal{Q}_l^{-1} \mathcal{Q}_l L &\geq 0 \xrightarrow{O \leq f_g^2} \begin{bmatrix} O_l & * \\ (L\mathcal{Q}_l)^{T} & \mathcal{Q}_l \end{bmatrix} \geq 0 \\ \left|u_q\right| &\leq d_q, \quad d_q > 0 \, (q = 1, \ldots, m) \\ &\rightarrow\rightarrow \begin{bmatrix} \omega_l & * \\ Y_l^{T} & \mathcal{Q}_l \end{bmatrix}, \\ \omega_{l,qq} &\leq d_q^2 \, (q = 1, \ldots, m) \end{aligned} \quad (50)$$

It can be proven that:

$$\begin{aligned} \left|F_l x_{\kappa+l|\kappa}\right|^2 \leq d_q^2 &\rightarrow \left\|Y_l \mathcal{Q}_l^{\frac{-1}{2}}\right\|^2 \left\|\mathcal{Q}_l^{-\frac{1}{2}} x_{\kappa+l|\kappa}\right\|^2 \\ &\leq f_g^2 \rightarrow \xrightarrow{\left\|\mathcal{Q}_l^{-\frac{1}{2}} x_{\kappa+l|\kappa}\right\|^2 \leq 1} \left\|Y_l \mathcal{Q}_l^{-\frac{1}{2}}\right\|^2 \\ &\leq d_q^2 \rightarrow Y_l \mathcal{Q}_l^{-\frac{1}{2}} \mathcal{Q}_l^{-\frac{1}{2}} Y_l^{T} \leq d_q^2 \rightarrow Y_l \mathcal{Q}_l^{-1} Y_l^{T} \\ &\leq d_q^2 d_q^2 - Y_l \mathcal{Q}_l^{-1} Y_l^{T} \geq 0 \xrightarrow{W_l \leq d_q^2} \begin{bmatrix} \omega_l & * \\ (Y_l)^{T} & \mathcal{Q}_l \end{bmatrix} \geq 0 \end{aligned}$$

Algorithm 1: In this part, we need to solve the following optimization problem at the time k :

$$\begin{aligned} &\min_{\Sigma_l, \partial} \partial \\ &s.t. \; (26) \; (34) \; (40) \; (41) \; (24) \; (49) \; (50) \\ &\quad \text{where } \sum\nolimits_l = \{Q_l, Y_l, \omega_l, O_l, \zeta_l\} \end{aligned} \quad (51)$$

If equation (51) is solved, the input of control at the current time of κ is $u_{\kappa+l|\kappa} = \tilde{F}_0 x_{\kappa+l|\kappa}$.

For the linear parameter variable system, a multi-stage control strategy is utilized; where F_l is predicted at time k as the feedback control gain at time $\kappa + l$ and $F_l = F_{N-1}$ when $l \geq N - 1$.

$$u_{\kappa} = F_l x_{\kappa} \quad (52)$$

The closed-loop system under control law equation (52) can be represented as:

$$\begin{aligned} x_{\kappa+l+1|\kappa} &= \sum_{i=1}^{r} \rho_{\kappa+l|\kappa,i} \left(\left(\tilde{\mathrm{A}}_i\right) x_{\kappa+l|\kappa} + (D_i)\, \omega_{\kappa+l|\kappa}\right) \\ z_{\kappa+l|\kappa} &= \sum_{i=1}^{r} \rho_{\kappa+l|\kappa,i} \left(\tilde{C}_i\right) x_{\kappa+l|\kappa} \\ \tilde{\mathrm{A}}_i &= A_i + B_i F_l \\ \tilde{C}_i &= \begin{bmatrix} C_i \\ R_i F_l \end{bmatrix} \end{aligned} \quad (53)$$

We need to choose a Lyapunov function $\left(x_{\kappa+l|\kappa}\right) = x_{\kappa+l|\kappa}^{T} P_l x_{\kappa+l|\kappa}, P_l > 0 \, (l = 0, \ldots, N-1)$ *when* $l \geq N - 1$, $P_l = P_{N-1}$. Similar to the proof in the reference [27] and lemma 3, we can prove the following result.

Lemma 5: With considering the LPV systems equation (9), the closed-loop system under the control law equation (52) satisfies the following conditions, (54), as shown at the bottom of the next page.

Let $\mathcal{Q}_l = \partial P_l^{-1}, F_l = Y_l \mathcal{Q}_l^{-1}, \bar{X}_{il}^{(11)} = \partial P_l^{-1} X_{il}^{(11)} P_l^{-1}$, $\bar{X}_{il}^{(12)} = \partial P_l^{-1} X_{il}^{(12)}$, $\bar{X}_{il}^{(22)} = \partial X_{il}^{(22)}$. Also, u by sing lemma 2 and lemma 4, equation (54) is equal to the following LMI:

$$\begin{bmatrix} \mathcal{Q}_l - \bar{X}_{il}^{(11)} & -\bar{X}_{il}^{(12)} & \divideontimes & \divideontimes & \divideontimes \\ -\bar{X}_{il}^{(21)} & \partial\varphi^2 - \bar{X}_{il}^{(22)} & \divideontimes & \divideontimes & \divideontimes \\ A_i\mathcal{Q}_l + B_i Y_l & \partial D_i & \zeta_{l+1} & \divideontimes & \divideontimes \\ C_i\mathcal{Q}_l & 0 & 0 & \partial I & \divideontimes \\ R_i Y_l & 0 & 0 & 0 & \partial I \end{bmatrix} \geq 0 \quad (55)$$

$$\begin{bmatrix} X_i^{(11)} & X_i^{(12)} \\ X_i^{(21)} & X_i^{(22)} \end{bmatrix} > 0 \quad (56)$$

Algorithm 2: We need to solve the following optimization issue at the time k :

$$\begin{aligned} &\min_{\Sigma_l, \partial} \partial \\ &s.t.\ \ (26)\ (40)\ (49)\ (50)\ (55)\ (56) \\ &\quad \text{where } \sum\nolimits_l = \{Q_l, Y_l, \omega_l, O_l, \zeta_l\} \end{aligned} \quad (57)$$

If equation (57) is solved, the input of control at the current time of κ is:

$$u_{\kappa+l|\kappa} = F_0 x_{\kappa+l|\kappa} \quad (58)$$

The process of implementing the proposed controller in MATLAB is shown in the following algorithm for a single-phase system. To control the other phases separately, the controller algorithm is implemented in the same way. To solve the inequality, YALMIP solver is used in MATLAB version 2019a. Codes for implementing the controller are as the following:

Define parameters of the system, controller and references
Get data from sensors
Calculate the error between measured data and reference
Controller:
Use YALMIP solver to solve and optimize equations 51 and 57 to retrieve control signal gains
Calculate the control signal based on the sum of feedback and backward control gains (equations 52 and 58)
Send a control signal to the system

III. CASE STUDY AND SIMULATION

A. PARAMETERS AND CASE STUDIES

In this section, the efficiency of the controller is evaluated under different load scenarios, including balanced or unbalanced resistive, inductive, and non-linear loads. Figure 4 displays an islanded MG with 2 DG units. Simulations have been performed by Matlab/Simulink.

The specifications of the power network and also control parameters are displayed in Table 1. As can be seen from Figure 4, the specifications of the system are measured to be utilized in the input of the controller.

According to Figure 4, the first DG is chosen as the control of voltage and frequency, which is responsible for regulating and adjusting the voltage and frequency of the MG in time of the system encounters every load variation. On the other hand, the second DG works in the mode of output current control, wherein gains have been utilized for sharing loads. The control signal has been utilized as the input of the PWM to control the inverter. A current load factor is also utilized as the reference current signal.

1) CASE A: SYMMETRICAL RESISTIVE LOAD

In this case, the efficiency of the proposed controller under symmetrical resistive load has been investigated. The values are also repeatedly stated in Table 2. In time t = 0.205 s symmetrical load is introduced into the system, respectively. It should be noted that the load value is assumed to be measurable and a load factor is utilized as the reference current signal.

Figure 5 depicts the simulation results. Figure 5 (a and d) illustrate the voltage of MG and also the zero steady-state error of phase voltage a. The presented algorithm effectively can track the reference signal with having a minimum error, which approves the robustness of the control strategy against linear load changing. The load current also utilized as the reference current signal, which is shown in Figure 5 (b). Besides, Figs. 5(c and e) display the reference signal and output current of the second DG and also the zero steady-state error of phase voltage a. Figure 5 (c and e) show the robustness of the provided current controller. The harmonic spectrum of voltage is analyzed and the amplitude of output voltage is 109.6 and the THD is 0.16 percent.

$$\begin{bmatrix} \hat{A} & \divideontimes \\ \left(\sum_{i=1}^{r} \rho_{\kappa+l|\kappa}(D_i)\right)^T P_{l+1} \left(\sum_{i=1}^{r} \rho_{\kappa+l|\kappa}(A_i + B_i F_l)\right) & \left(\sum_{i=1}^{r} \rho_{\kappa+l|\kappa}(D_i)\right)^T P_{l+1} \left(\sum_{i=1}^{r} \rho_{\kappa+l|\kappa}(D_i)\right) - \varphi^2 I \end{bmatrix}$$
$$\leq - \begin{bmatrix} \rho_{\kappa+l|\kappa} x_{\kappa+l|\kappa} \\ \rho_{\kappa+l|\kappa} x_{\kappa+l|\kappa} \end{bmatrix}^T \begin{bmatrix} X_i^{(11)} & X_i^{(12)} \\ X_i^{(21)} & X_i^{(22)} \end{bmatrix} \begin{bmatrix} \rho_{\kappa+l|\kappa} x_{\kappa+l|\kappa} \\ \rho_{\kappa+l|\kappa} x_{\kappa+l|\kappa} \end{bmatrix}$$
$$\hat{A} = \left(\sum_{i=1}^{r} \rho_{\kappa+l|\kappa,i}(A_i + B_i F_l)\right)^T P_{l+1} \left(\sum_{i=1}^{r} \rho_{\kappa+l|\kappa,i}(A_i + B_i F_l)\right) - P_l + \left(\sum_{i=1}^{r} \rho_{\kappa+l|\kappa,i} \begin{bmatrix} C_i \\ R_i F_l \end{bmatrix}\right)^T P_{l+1} \left(\sum_{i=1}^{r} \rho_{\kappa+l|\kappa,i} \begin{bmatrix} C_i \\ R_i F_l \end{bmatrix}\right) \quad (54)$$

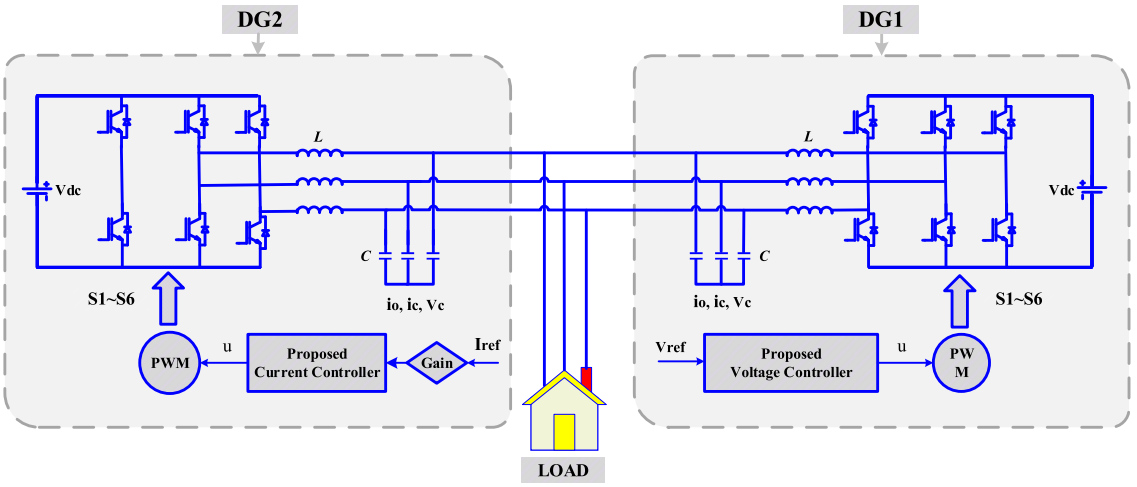

FIGURE 4. Simulated microgrid system consisting of two DG units with the proposed controller.

TABLE 1. Parameters of the proposed controller and the DGs.

Distributed Generation Unit	Symbol	Quantity	Value
Voltage-frequency controller unit (DG1)	V_{DC}	DC voltage input	800 V
	ω_r	Voltage angular frequency	377 Rad/s
	L	Filter inductive	11 mH
	f	Switching frequency	15 kHZ
	V_{ref}	Reference voltage signal	110 $\sin(2\pi 60)$
Current controller units (DG2)	V_{DC}	DC input voltage	800 V
	L	Inductive filter	11 mH
	C	Capacitor filter	220 µF
	I_{max}	Maximum production current of DG	25 A
	f	Switching frequency	15 kHz
Controller parameters	ω_l		0.3
	∂		1

TABLE 2. Balanced resistive load characteristics.

Variables	Initial load (Ω)	Balance load (Ω)	Unbalance load (Ω)	Inductive load		Non-linear load	
				Ω	mH	Ω	µF
Phase a	40	2	2	2	100	100	5
Phase b	40	2	1.5	2	100		
Phase c	40	2	2.5	2	100		

2) CASE B: RESISTIVE UNBALANCED LOAD

In this case, the efficiency of the proposed controller under resistive unbalance load has been investigated. The values are also repeatedly stated in Table 2. In time $t = 0.405\ s$ asymmetric load is introduced into the system. It should be noted that the load value is assumed to be measurable and a load factor is utilized as the reference current signal.

Figure 6 depicts the simulation results. Figure 6 (a and d) illustrate the voltage of MG and also the zero steady-state error of phase voltage a. The presented algorithm effectively can track the reference signal with having a minimum error, which approves the robustness of the control strategy against linear load changing. The load current also utilized as the reference current signal which is shown in Figure 6 (b). Besides, Figure 6 (c and e) display the reference signal and output current of the second DG and also the zero steady-state error of phase voltage a. Figure 6 (c and e) show the robustness of the provided current controller. The harmonic spectrum of voltage is analyzed and the amplitude of output voltage is 109.5 and the THD is 0.16 percent.

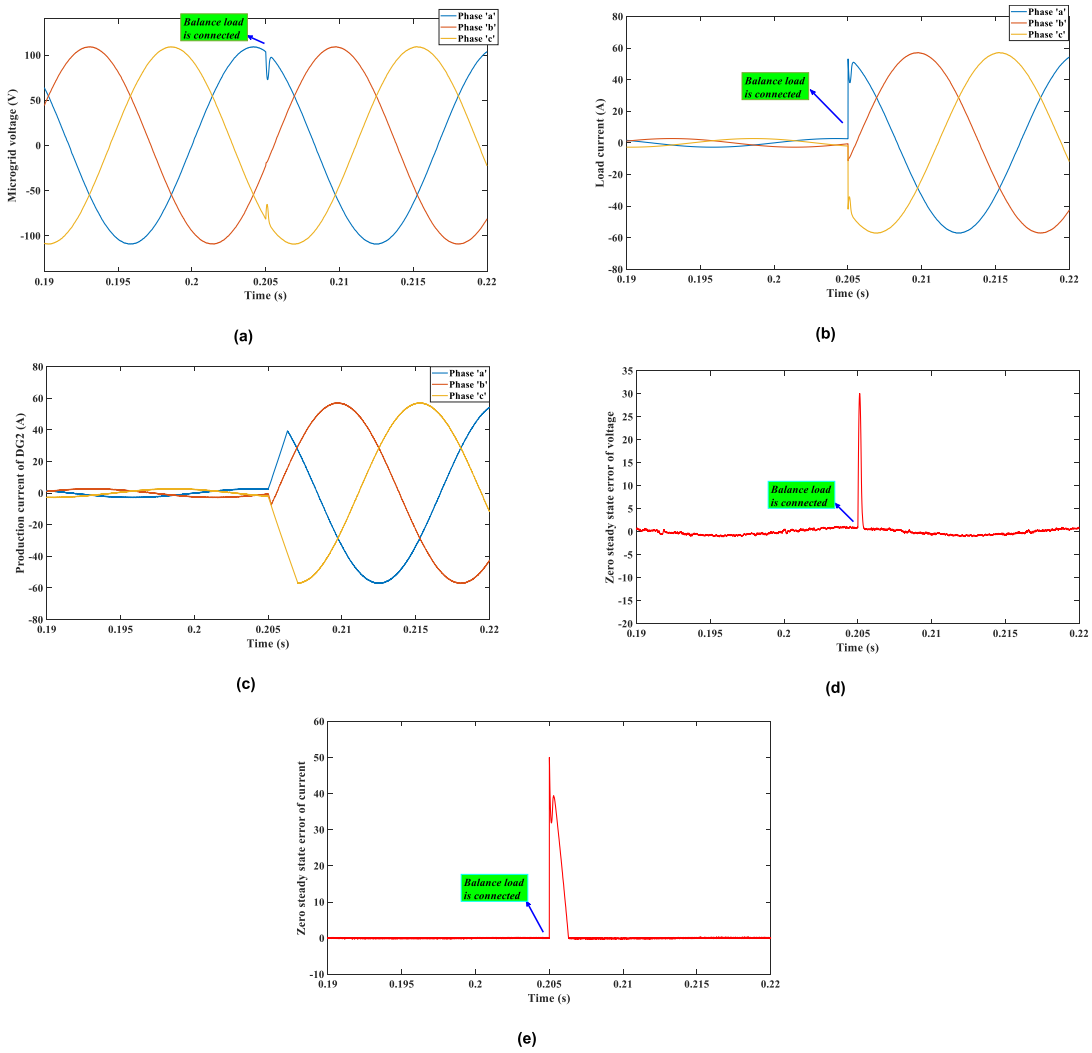

FIGURE 5. The results of the simulation for the presented controller under resistive balance load: (a) MG voltage; (b) load current; (c) current of generation for the second DG; (d) zero steady-state error of phase voltage a; (e) zero steady-state error of phase current *a*.

TABLE 3. Steady-state simulation results of output phase voltage *a*.

Controller	Load type	Output voltage peak	THD (%)	Robustness
Proposed controller	Balanced Resistive Load	109.6	0.16 %	Very good
	Unbalanced Resistive Load	109.5	0.16 %	
	Inductive Load	109.5	0.18 %	
	Nonlinear Load	109.5	0.19 %	
Classic sliding mode controller [28]	Balanced Resistive Load	106	0.46 %	Good
	Unbalanced Resistive Load	106	0.52 %	
	Inductive Load	105.8	0.59 %	
	Nonlinear Load	106.3	0.73 %	
Classic back stepping controller [29]	Balanced Resistive Load	102.7	0.55 %	Good
	Unbalanced Resistive Load	102.7	0.54 %	
	Inductive Load	102.6	0.52 %	
	Nonlinear Load	102.6	0.55 %	

3) CASE C: INDUCTIVE LOAD

In this case, the efficiency of the proposed controller under inductive load has been investigated. The values are also repeatedly stated in Table 2. At time $t = 0.6$ s inductive load is introduced into the system. It should be noted that the load value is assumed to be

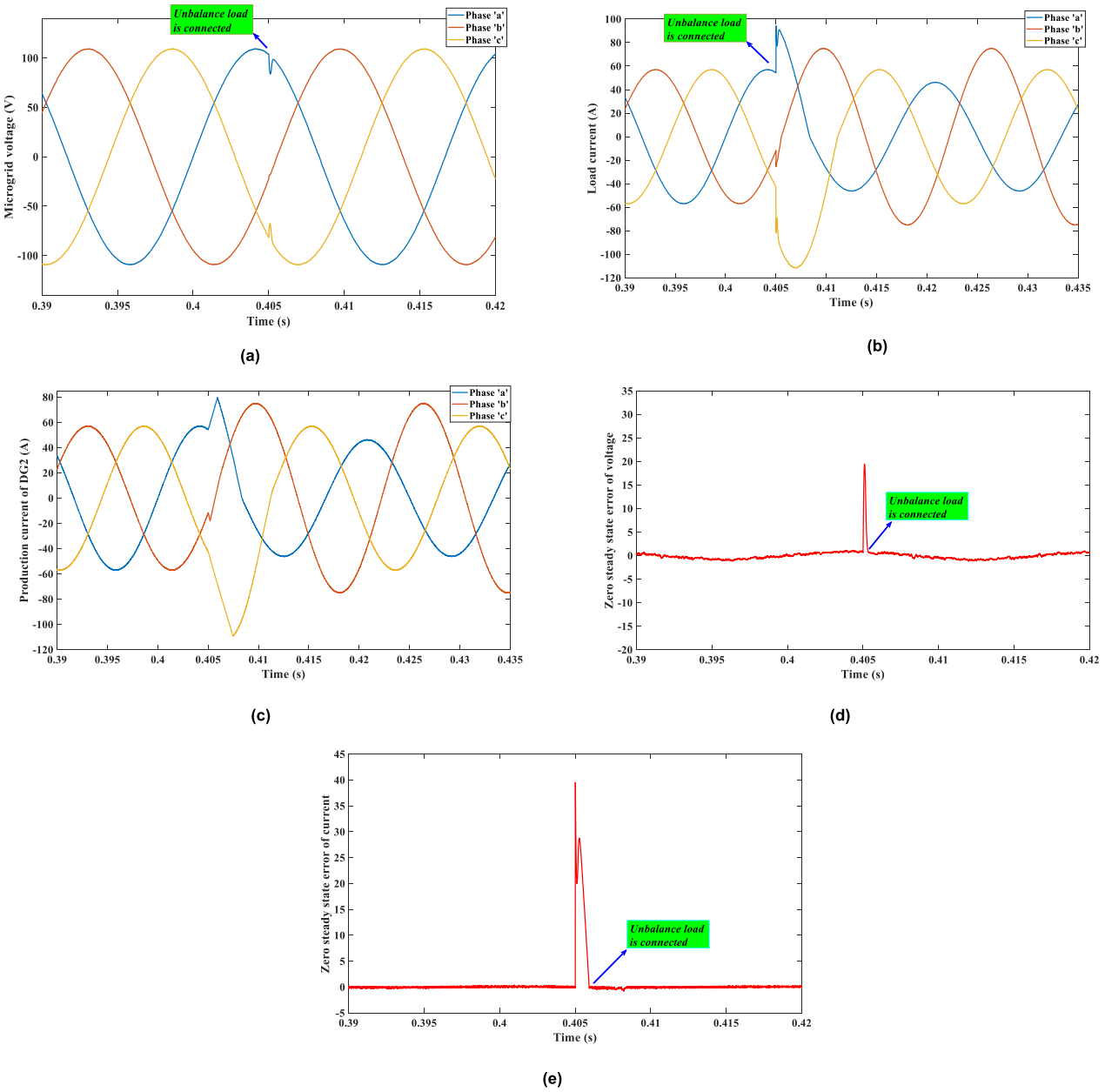

FIGURE 6. The results of the simulation for the presented controller under resistive asymmetric load: (a) MG voltage; (b) load current; (c) current of generation for the second DG; (d) zero steady-state error of phase voltage a; (e) zero steady-state error of phase current *a*.

measurable and a load factor is utilized as the reference current signal.

Figure 7 depicts the simulation results. Figure 7 (a and d) illustrate the voltage of MG and also the zero steady-state error of phase voltage a. The presented algorithm effectively can track the reference signal with having a minimum error, which approves the robustness of the control strategy against linear load changing. The load current is also utilized as the reference current signal which is shown in Figure 7 (b).

Besides, Figure 7 (c and e) display the reference signal and output current of the second DG and also the zero steady-state error of phase voltage a. Figure 7 (c and e) show the robustness of the provided current controller. The harmonic spectrum of voltage is analyzed. The amplitude of output voltage is 109.5 and the THD is 0.18 percent.

4) CASE D: NON-LINEAR LOAD

In case B, the efficiency of the presented controller under non-linear loads will be examined. The values are repeatedly stated in Table 2. At time t = 0.4 s, a non-linear load is applied to the system. It has to be noted that the load value is assumed to be measurable and a load factor is utilized as the reference current signal.

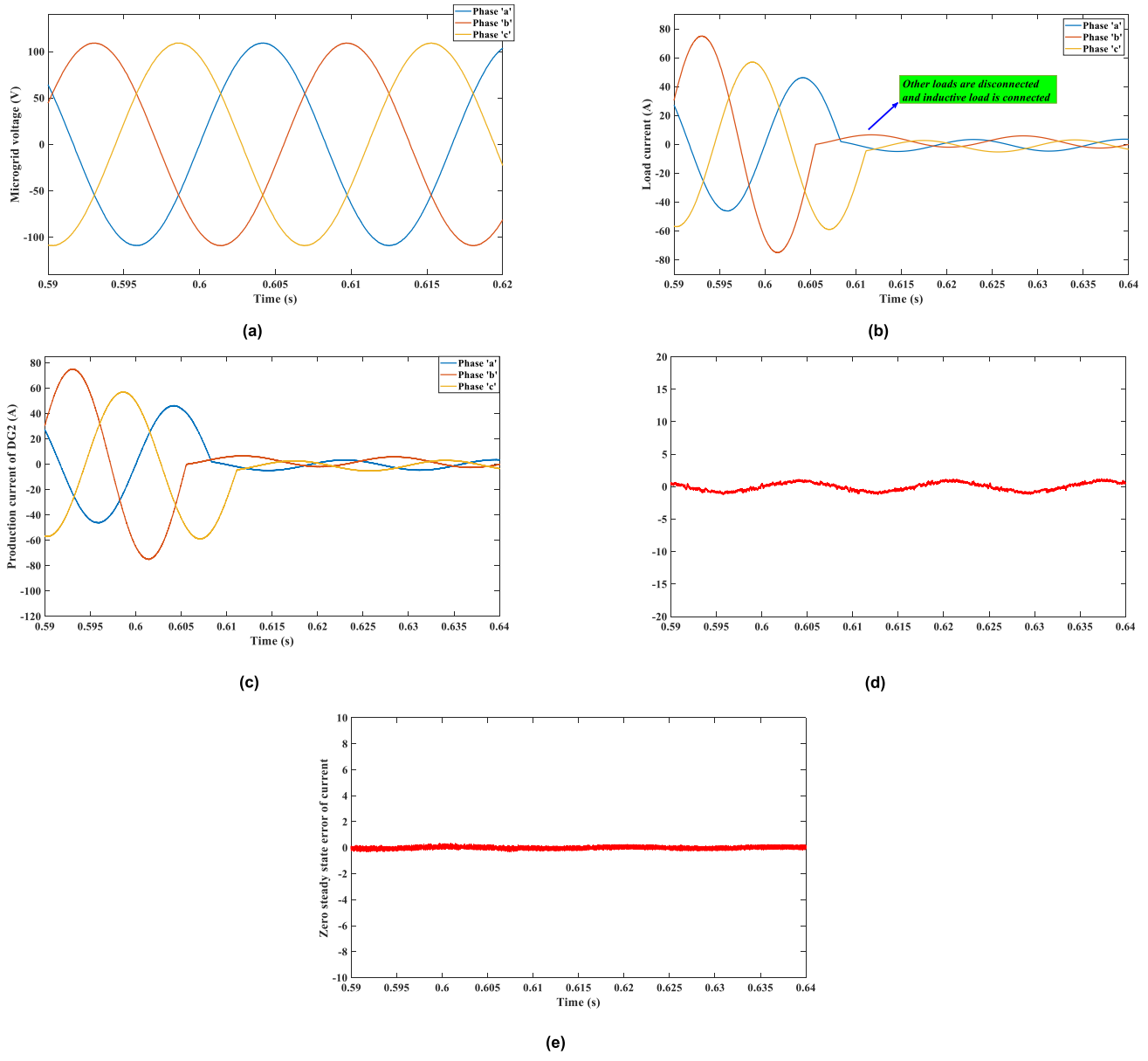

FIGURE 7. The results of the simulation for the presented controller under resistive asymmetric load: (a) MG voltage; (b) load current; (c) current of generation for the second DG; (d) zero steady-state error of phase voltage a; (e) zero steady-state error of phase current *a*.

Figure 8 depicts the results of the simulation. Figure 8 (a and d) demonstrate the voltage of MG and the zero steady-state error of phase voltage a. It is evident that the presented algorithm, in this case, is effectively able to track the reference signal with minimum error, which approves the robustness of the control strategy against linear load changing. The load current used as the reference current signal is shown in Figure 8 (b). Moreover, Figure 8 (c and e) display the reference signal and output current of the second DG and the zero steady-state error of phase voltage a. Figure 8 (c and e) show the robustness of the presented current controller. The harmonic spectrum of voltage is depicted in Figure 8 (f); as can be seen, the amplitude of output voltage is 109.5 and the THD is 0.19 percent.

B. COMPARISON WITH OTHER CONTROLLERS

In this part, the efficiency of the provided controller is compared with the classic sliding mode controller and the classic backstepping controller in Table 3. The presented controller can give improved output peak voltage and THD; besides, it can decrease steady-state error in comparison with the classic non-linear controller. To have a better comparison with the suggested controller, details of sliding mode and back stepping controllers are extracted from

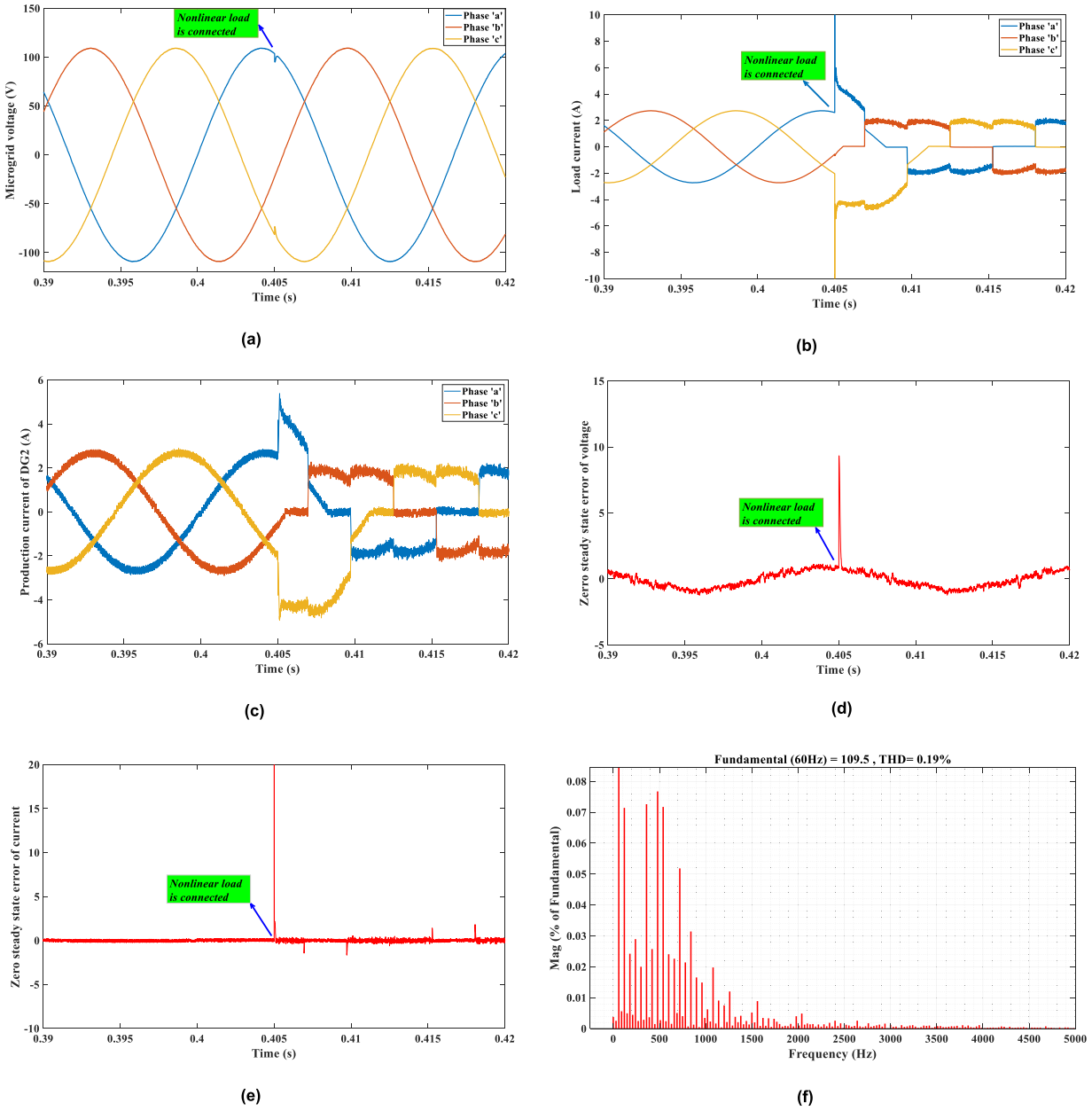

FIGURE 8. Results of the simulation for the presented controller under non-linear load: (a) MG voltage; (b) load current; (c) generation current of the second DG; (d) zero steady-state error of phase voltage a; (e) zero steady-state error of phase current a; (f) Harmonic spectrum of voltage.

references [28] and [29] and implemented controllers on the system, which are shown in Figure 4.

IV. CONCLUSION

In this article, we proposed a concept model prediction and H_2/H_∞ control plan with input and state constraints with considering disturbances in an MG with two DGs. The model predictive control has used both H_2 and H_∞ to optimize the concept; and a gain-scheduled MPC, H_2/H_∞ algorithm was also studied using LMI techniques. Considering proper upper boundaries as LMI auxiliary variables in terms of stability analysis leads to a reduction in conservatism. The presented algorithm provides a faster response and is added to the controller to avoid obstacles in an algorithmic way like the switching algorithm. Additionally, closed-loop stability and recursive feasibility of the proposed model predictive control have been proven. The main advantages of the proposed approach are the existence of a control law for all conditions concerning the linear and non-linear loads and the ability to avoid obstacles, and decreasing the impacts of disturbances. Not only that, but it was demonstrated that the proposed controller is able to track the reference signal with a minimum steady-state error. Besides, using the presented controller has proven that it can develop the results of the

steady-state of the controller, including output voltage peak, RMS, and THD. Obtained simulation results demonstrated that the presented controller is robust against variable load situations. Considering the obtained results, the controller is insensitive to changes in the phase and amplitude of the reference signal. This controller has a decent and fast response to the reference variations and its steady-state error is negligible.

REFERENCES

[1] G. Turner, J. P. Kelley, C. L. Storm, D. A. Wetz, and W.-J. Lee, "Design and active control of a microgrid testbed," *IEEE Trans. Smart Grid*, vol. 6, no. 1, pp. 73–81, Jan. 2015.

[2] Z. Wang, U. Munawar, and R. Paranjape, "Stochastic optimization for residential demand response with unit commitment and time of use," *IEEE Trans. Ind. Appl.*, vol. 57, no. 2, pp. 1767–1778, Mar. 2021.

[3] M. Ghiasi, T. Niknam, M. Dehghani, P. Siano, H. H. Alhelou, and A. Al-Hinai, "Optimal multi-operation energy management in smart microgrids in the presence of RESs based on multi-objective improved DE algorithm: Cost-emission based optimization," *Appl. Sci.*, vol. 11, no. 8, p. 3661, Apr. 2021.

[4] M. Ghiasi, M. Dehghani, T. Niknam, H. R. Baghaee, S. Padmanaban, G. B. Gharehpetian, and H. Aliev, "Resiliency/cost-based optimal design of distribution network to maintain power system stability against physical attacks: A practical study case," *IEEE Access*, vol. 9, pp. 43862–43875, 2021.

[5] M. Ghiasi, M. Dehghani, T. Niknam, A. Kavousi-Fard, P. Siano, and H. H. Alhelou, "Cyber-attack detection and cyber-security enhancement in smart DC-microgrid based on blockchain technology and Hilbert Huang transform," *IEEE Access*, vol. 9, pp. 29429–29440, 2021.

[6] M. Dehghani, M. Ghiasi, T. Niknam, A. Kavousi-Fard, M. Shasadeghi, N. Ghadimi, and F. Taghizadeh-Hesary, "Blockchain-based securing of data exchange in a power transmission system considering congestion management and social welfare," *Sustainability*, vol. 13, no. 1, p. 90, Dec. 2020.

[7] S. V. Iyer, M. N. Belur, and M. C. Chandorkar, "A generalized computational method to determine stability of a multi-inverter microgrid," *IEEE Trans. Power Electron.*, vol. 25, no. 9, pp. 2420–2432, Sep. 2010.

[8] H. Z. Maia, J. O. P. Pinto, and E. A. A. Coelho, "Power response optimization of inverter grid parallel operation using V-ω and QV curves, and phase feedback based on genetic algorithm," in *Proc. 33rd Annu. Conf. IEEE Ind. Electron. Soc. (IECON)*, Nov. 2007, pp. 1679–1684.

[9] J. Steenis, K. Tsakalis, and R. Ayyanar, "Robust control of an islanded microgrid," in *Proc. 38th Annu. Conf. IEEE Ind. Electron. Soc. (IECON)*, Oct. 2012, pp. 2447–2451.

[10] J. Steenis, L. Breazeale, K. Tsakalis, and R. Ayyanar, "H_∞ and gain scheduled H_∞ control for islanded microgrids," in *Proc. IEEE Energy Convers. Congr. Expo.*, Sep. 2013, pp. 4603–4608.

[11] J. Steenis, K. Tsakalis, and R. Ayyanar, "An approach to bumpless control for LPV modeled inverters in a microgrid," *IEEE Trans. Power Electron.*, vol. 29, no. 11, pp. 6214–6223, Nov. 2014.

[12] M. Ghiasi, "Detailed study, multi-objective optimization, and design of an AC-DC smart microgrid with hybrid renewable energy resources," *Energy*, vol. 169, pp. 496–507, Feb. 2019.

[13] S.-Y. Cheong and M. G. Safonov, "Slow-fast controller decomposition bumpless transfer for adaptive switching control," *IEEE Trans. Autom. Control*, vol. 57, no. 3, pp. 721–726, Mar. 2012.

[14] C. Olalla, R. Leyva, I. Queinnec, and D. Maksimovic, "Robust gain-scheduled control of switched-mode DC-DC converters," *IEEE Trans. Power Electron.*, vol. 27, no. 6, pp. 3006–3019, Jun. 2012.

[15] M. Pasamontes, J. D. Álvarez, J. L. Guzmán, and M. Berenguel, "Bumpless switching in control—A comparative study," in *Proc. IEEE 15th Conf. Emerg. Technol. Factory Automat. (ETFA)*, Sep. 2010, pp. 1–8.

[16] Z. Li, Z. Cheng, S. Li, J. Si, J. Gao, W. Dong, and H. S. Das, "Virtual synchronous generator and SMC based cascaded control for voltage-source grid-supporting inverters," *IEEE J. Emerg. Sel. Topics Power Electron.*, early access, Feb. 2, 2021, doi: 10.1109/JESTPE.2021.3056576.

[17] X. Meng, J. Liu, and Z. Liu, "A generalized droop control for grid-supporting inverter based on comparison between traditional droop control and virtual synchronous generator control," *IEEE Trans. Power Electron.*, vol. 34, no. 6, pp. 5416–5438, Jun. 2019.

[18] W. Jiang and B. Fahimi, "Active current sharing and source management in fuel cell–battery hybrid power system," *IEEE Trans. Ind. Electron.*, vol. 57, no. 2, pp. 752–761, Feb. 2010.

[19] D.-E. Kim and D.-C. Lee, "Feedback linearization control of three-phase UPS inverter systems," *IEEE Trans. Ind. Electron.*, vol. 57, no. 3, pp. 963–968, Mar. 2010.

[20] G. Escobar, P. Mattavelli, A. M. Stankovic, A. A. Valdez, and J. Leyva-Ramos, "An adaptive control for UPS to compensate unbalance and harmonic distortion using a combined capacitor/load current sensing," *IEEE Trans. Ind. Electron.*, vol. 54, no. 2, pp. 839–847, Apr. 2007.

[21] R.-J. Wai and C.-Y. Lin, "Active low-frequency ripple control for clean-energy power-conditioning mechanism," *IEEE Trans. Ind. Electron.*, vol. 57, no. 11, pp. 3780–3792, Nov. 2010.

[22] M. Dehghani, M. H. Khooban, T. Niknam, and S. M. R. Rafiei, "Time-varying sliding mode control strategy for multibus low-voltage microgrids with parallel connected renewable power sources in islanding mode," *J. Energy Eng.*, vol. 142, no. 4, Dec. 2016, Art. no. 05016002.

[23] M. Dehghani, T. Niknam, M.-R. Tavana, and G. Asadi, "A rotating reference signal based on nonlinear control for multi-bus single phase microgrids," *Universal J. Control Automat.*, Vol. 4, no. 3, pp. 29–41, doi: 10.13189/ujca.2016.040302.

[24] L. F. A. Pereira, J. V. Flores, G. Bonan, D. F. Coutinho, and J. M. G. da Silva, "Multiple resonant controllers for uninterruptible power supplies—A systematic robust control design approach," *IEEE Trans. Ind. Electron.*, vol. 61, no. 3, pp. 1528–1538, Mar. 2013.

[25] L. A. Maccari, J. R. Massing, L. Schuch, C. Rech, H. Pinheiro, R. C. L. F. Oliveira, and V. F. Montagner, "LMI-based control for grid-connected converters with LCL filters under uncertain parameters," *IEEE Trans. Power Electron.*, vol. 29, no. 7, pp. 3776–3785, Jul. 2014.

[26] Y.-Y. Cao, Z. Lin, and Y. Shamash, "Set invariance analysis and gain-scheduling control for LPV systems subject to actuator saturation," *Syst. Control Lett.*, vol. 46, no. 2, pp. 137–151, Jun. 2002.

[27] H. Lim, Y. Kang, C. Kim, J. Kim, and B.-J. You, "Non-linear model predictive controller design with obstacle avoidance for a mobile robot," in *Proc. IEEE/ASME Int. Conf. Mechtronic Embedded Syst. Appl.*, Oct. 2008, pp. 494–499.

[28] J. Gao, Z. Sun, D. Li, W. Zhou, and C. Chen, "A novel robust adaptive control of parallel energy resources in smart island," *Int. J. Electr. Power Energy Syst.*, vol. 128, Jun. 2021, Art. no. 106703.

[29] O. Diouri, N. Es-Sbai, F. Errahimi, A. Gaga, and C. Alaoui, "Control of single phase inverter using back-stepping in stand-alone mode," in *Proc. Int. Conf. Wireless Technol., Embedded Intell. Syst. (WITS)*, Apr. 2019, pp. 1–6.

MOSLEM DEHGHANI was born in Shiraz, Iran, in 1990. He received the B.S. and M.S. degrees in electrical engineering from Islamic Azad University–Kazerun Branch, in 2012 and 2014, respectively, and the Ph.D. degree in electrical engineering from the Shiraz University of Technology, Shiraz, in 2019. His current research interests include power electronic, control, and cyber security analysis of smart grids, microgrid, smart city, HVDC systems and protection of power systems, fuzzy logic, and signal processing

MOHAMMAD GHIASI (Member, IEEE) is currently pursuing the Ph.D. degree with the University of Regina, Regina, Saskatchewan, Canada. Since 2018, he has been a Research Assistant with the Shiraz University of Technology, Shiraz, Iran. His research interests include modeling, simulation and optimization of power systems, integration and control of hybrid and distributed renewable energy resources, smart grids, and cyber-physical resilience in power systems has led to multiple publications in these fields. He has been serving as the guest editor for several special issues in various scientific ISI ranked journals. He is also the volunteer reviewer for several IEEE, IET, Elsevier, Springer, Wiley, Sage, MDPI and Taylor and Francis journals and conferences.

TAHER NIKNAM (Senior Member, IEEE) was born in Shiraz, Iran. He received the B.S. degree in power electrical engineering from Shiraz University, Shiraz, in 1998, and the M.S. and Ph.D. degrees in power electrical engineering from the Sharif University of Technology, Tehran, Iran, in 2000 and 2005, respectively. He is currently a Faculty Member with the Electrical Engineering Department, Shiraz University of Technology. His research interests include power system restructuring, impact of distributed generations on power systems, optimization methods, and evolutionary algorithms.

KUMARS ROUZBEHI (Senior Member, IEEE) received the Ph.D. degree in electric energy systems from the Technical University of Catalonia (UPC), Barcelona, Spain, in 2016.

Prior to this, he was a Academic Staff with the Faculty of Electrical Engineering, Islamic Azad University (IAU), Iran, from 2002 to 2011. In parallel with teaching and research with IAU, he was the CEO of Khorasan Electric and Electronics Industries Research Company, from 2004 to 2010. From 2017 to 2019, he was an Associate Professor with Loyola Andalucía University, Seville, Spain. In 2019, he joined the Department of Systems and Automatic Control Engineering, University of Seville, Seville. He holds a patent in AC grid synchronization of voltage source power converters. He has authored or coauthored almost 100 technical books, book chapters, journal articles, and technical conference proceedings.

Dr. Rouzbehi has been a TPC Member of the International Conference on Electronics, Communication, Control, and Power Engineering (IEEE-ECCP), since 2014, a Scientific Board Member of the (IEA) International Conference on Technology and Energy Management, since 2015, and a TPC Member of COMPEL 2020. He is an Associate Editor of the IEEE Systems Journal, *IET Generation, Transmission and Distribution*, *IET Renewable Power Generation*, *High Voltage* (IET), and *IET Energy Systems Integration*. He was a recipient of the Second Best Paper Award 2015 from the IEEE Power Electronics Society and the IEEE Journal of Emerging and Selected Topics in Power Electronics.

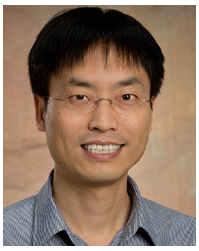

ZHANLE WANG (Member, IEEE) received the B.Eng. degree in industrial automation from the North China University of Science and Technology, Tangshan, China, in 2001, and the M.Sc. and Ph.D. degrees in electronic systems engineering from the University of Regina, Regina, SK, Canada, in 2012 and 2015, respectively.

Since 2016, he has been with the Faculty of Engineering and Applied Science, University of Regina, where he is currently an Assistant Professor. His research interests include computational methods for smart grids and energy systems integration; integration of distributed energy resources, such as electric vehicles, demand response, energy storage, and small scale solar/wind power; simulation and modeling optimal control of electricity usage; vehicle-to-grid systems (V2G); renewable energy integration; optimization theory and applications; and multi-agent systems. He has been serving as the Executive Committee for IEEE South Saskatchewan Section, since 2016, where he is the Chair of professional activities.

PIERLUIGI SIANO (Senior Member, IEEE) received the M.Sc. degree in electronic engineering and the Ph.D. degree in information and electrical engineering from the University of Salerno, Salerno, Italy, in 2001 and 2006, respectively.

He is currently a Professor and the Scientific Director of the Smart Grids and Smart Cities Laboratory, Department of Management and Innovation Systems, University of Salerno. Since 2021, he has been a Distinguished Visiting Professor with the Department of Electrical and Electronic Engineering Science, University of Johannesburg. His research interests include demand response, on energy management, on the integration of distributed energy resources in smart grids, on electricity markets, and on planning and management of power systems. In these research fields, he has coauthored more than 650 articles, including more than 370 international journal articles that received in Scopus more than 12700 citations with an H-index equal to 55. In 2019, 2020, and 2021, he has been awarded as a Highly Cited Researcher in engineering by the Web of Science Group. He has been the Chair of the IES TC on Smart Grids. He is an Editor of the Power and Energy Society Section of IEEE Access, the IEEE Transactions on Power Systems, the IEEE Transactions on Industrial Informatics, the IEEE Transactions on Industrial Electronics, the IEEE Systems Journal, the IEEE Open Journal of the Industrial Electronics Society, *IET Smart Grid*, and *IET Renewable Power Generation*.

HASSAN HAES ALHELOU (Senior Member, IEEE) is currently a Faculty Member with Tishreen University, Lattakia, Syria, and a Consultant with Sultan Qaboos University (SQU), Oman. He is also with Monash University, Melbourne, Australia. He was a Senior Researcher with University College Dublin (UCD), Ireland. He is included in the 2018 and 2019 Publons list of the top 1% best reviewer and researchers in the field of engineering. He has published more than 160 research papers in the high quality peer-reviewed journals and international conferences. He has also performed more than 6000 reviews for high prestigious journals, including IEEE Transactions on Power Systems, IEEE Transactions on Smart Grids, IEEE Transactions on Industrial Informatics, IEEE Transactions on Industrial Electronics, *Energy Conversion and Management*, *Applied Energy*, and *International Journal of Electrical Power and Energy Systems*. He has participated in more than 15 industrial projects. His research interests include power systems, power system dynamics, power system operation and control, dynamic state estimation, frequency control, smart grids, micro-grids, demand response, load shedding, and power system protection. He was a recipient of the Outstanding Reviewer Award from *Energy Conversion and Management* journal, in 2016, *ISA Transactions* journal, in 2018, *Applied Energy* journal, in 2019, and many other Awards. He was a recipient of the Best Young Researcher in the Arab Student Forum Creative among 61 researchers from 16 countries at Alexandria University, Egypt, in 2011.